

Spherical excision for moving black holes and summation by parts for axisymmetric systems

Gioel Calabrese and David Neilsen

*Department of Physics and Astronomy, Louisiana State University,
202 Nicholson Hall, Baton Rouge, Louisiana 70803-4001*

(Dated: August 9, 2018)

It is expected that the realization of a convergent and long-term stable numerical code for the simulation of a black hole inspiral collision will depend greatly upon the construction of stable algorithms capable of handling smooth and, most likely, time dependent boundaries. After deriving single grid, energy conserving discretizations for axisymmetric systems containing the axis of symmetry, we present a new excision method for moving black holes using multiple overlapping coordinate patches, such that each boundary is fixed with respect to at least one coordinate system. This multiple coordinate structure eliminates all need for extrapolation, a commonly used procedure for moving boundaries in numerical relativity.

We demonstrate this excision method by evolving a massless Klein-Gordon scalar field around a boosted Schwarzschild black hole in axisymmetry. The excision boundary is defined by a spherical coordinate system co-moving with the black hole. Our numerical experiments indicate that arbitrarily high boost velocities can be used without observing any sign of instability.

I. INTRODUCTION

Inspiring black holes are among the strongest astrophysical sources of gravitational radiation. The expectation that such systems may soon be studied with gravitational wave detectors has focused attention on solving Einstein's equations for predictions of gravitational wave content. Although the Einstein equations present several unique challenges to the numerical relativist [1], on several of which we do not elaborate here, black holes present one particular additional challenge: they contain physical curvature singularities. While the infinities of the gravitational fields associated with this singularity cannot be represented directly on a computer, the spacetime near the black hole must be given adequately to preserve the proper physics.

Different strategies have thus been developed to computationally represent black holes, while removing the singularity from the grid. One method exploits the gauge freedom of general relativity by choosing a time coordinate that advances normally far from a singularity, slows down as a singularity is approached, and freezes in the immediate vicinity. Coordinates with this property are "singularity avoiding" [2, 3, 4]. While singularity avoiding coordinates have some advantages, one potential disadvantage is that the hypersurfaces of constant time may become highly distorted, leading to large gradients in the metric components. These slice-stretching (or "grid-stretching") effects, however, can be partially avoided through an advantageous combination of lapse and shift conditions. For example, long-term evolutions of single black holes have been reported by Alcubierre et al. [5]. Singularity avoiding slicings may be combined with black hole excision, a second method for removing the singularities from the computational domain. Currently, long-term binary black hole evolutions have only been performed using both techniques together.

Excision is based on the physical properties of event

horizons and the expectation that singularities always form within such horizons, and thus cannot be seen by distant observers, as formulated by the Cosmic Censor Conjecture [6]. As no future-directed causal curve connects events inside the black hole to events outside, Unruh proposed that one could simply remove the black hole from the computational domain, leaving the exterior computation unaffected [7]. Thus the black hole singularity is removed by placing an inner boundary on the computational domain at or within the event horizon. Excision has been extensively used in numerical relativity in the context of Cauchy formulations [8, 9, 10, 11, 12, 13, 14, 15, 16, 17, 18]. In particular, excision with moving boundaries, which is the primary focus of this paper, was explored in [14, 15, 16, 17, 18].

The physical principles that form the basis of excision make the idea beautiful in its simplicity. Translating them into a workable numerical recipe for black hole evolutions, on the other hand, requires some attention to detail. Two general questions arise regarding the implementation of excision, (1) Where and how to define the inner boundary? and (2) How to move the boundary? The first question applies to all excision algorithms, while the last question is specific to implementations where the excision boundary moves with respect to the grid. In addressing these questions we assume a symmetric (or at least strongly) hyperbolic formulation [19]. This is because excision fundamentally relies on the characteristic structure of the Einstein equations near event horizons, a structure which can only be completely defined and understood for strongly and symmetric hyperbolic sets of equations.

The first question involves several considerations, including the location of the boundary, its geometry, and its discrete representation. The requirement that all modes at the excision boundary are leaving the computational domain can be non trivial. It may appear that this condition would be satisfied simply by choosing any boundary

within the event horizon (or, for practical purposes, the apparent horizon). However, the outflow property of the excision boundary depends on the characteristic speeds of the system in the normal directions to the boundary. For example, in the analytic Schwarzschild solution, assuming that the system has characteristic speeds bounded by the light cone, a spherical boundary can be excised at $r \leq 2M$. A cubical boundary, on the other hand, imposes an onerous restriction on the excision volume: in Cartesian Kerr–Schild coordinates the faces of a cube centered on the black hole must be less than $4\sqrt{3}/9M \approx 0.7698M$ in length [13, 20]. Remarkably, as was first noticed by Lehner [21], for the rotating Kerr solution in Kerr–Schild coordinates a well-defined cubical excision boundary is impossible for interesting values of the spin parameter. (See the appendix for further discussion.) Whereas with a pseudospectral collocation method the implementation of a smooth spherical excision boundary is trivial [22], this is generally not the case for finite differencing. As may be expected, smooth boundaries, which can be adapted to the spacetime geometry, allow the excision boundary to be as far from the singularity as possible, making the most efficient use of the technique.

The discrete representation of boundaries can be a delicate issue, especially in numerical relativity where many large-scale finite difference computations are done in Cartesian coordinates. We focus our attention on smooth boundaries that may be defined as a constant value in the computational coordinates, e.g., $r = r_0$ in spherical coordinates describes a simple spherical boundary. The importance of accurately representing smooth boundaries has been demonstrated for the Euler equations, for example, by Dadone and Grossman for finite volume methods [23], and Bassi and Rebay [24] using finite elements. Bassi and Rebay studied high resolution planar fluid flow around a cylinder. They report spurious entropy production near the cylinder wall, which corrupts the solution even on extremely refined grids, when the cylindrical boundary is approximated by a polygon. Furthermore, in the conformal field equations approach to general relativity, a smooth boundary is required to avoid uncontrollable numerical constraint violation [25].

The second question applies to excision boundaries that move with respect to the grid. When the inner boundary moves, points that previously were excised enter the physical part of the grid, and must be provided with physical data for all fields. In recently proposed excision algorithms, these data are obtained by extrapolating the solution from the physical domain of the calculation. Numerical experiments have indicated that the stability of the method is very sensitive to the details of the extrapolation, see e.g., Ref. [16, 17, 26]. To examine the black hole excision problem with moving inner boundaries, we adopt an approach with some unique features. The heart of our method for moving excision is to use multiple coordinate patches such that each boundary is at a fixed location in one coordinate system. Adapting

coordinate patches to the boundary geometry allows us to excise as far from the singularity as possible and simplifies the determination of the outflow character of the excision boundary. The motion of the boundaries is incorporated through the relationships among the various coordinate systems. The grids representing the different coordinate patches overlap and communicate via interpolation. This technique is an extension of the one used in well-posedness proofs for problems in general domains (see Sec. 13.4 of [27]). In this paper we demonstrate the algorithm by solving the massless Klein-Gordon equation on a fixed, boosted Schwarzschild background. We find that the algorithm is stable for (apparently) all values of the boost parameter, $\beta = v/c$, and present results here showing stable evolutions for several cases with $\beta \leq 0.95$.

We specialize to axially symmetric spacetimes to reduce the computational requirements for our single-processor code. Axially symmetric spacetimes have sometimes been avoided in numerical relativity, with notable exceptions, see e.g., [28], owing to the difficulties in developing stable finite difference equations containing the axis of symmetry. In this paper we further present finite differencing methods for the wave equation in axially symmetric spacetimes in canonical cylindrical and spherical coordinates. These differencing schemes are second order accurate and their stability for a single grid is proved using the energy method [27]. Maximally dissipative boundary conditions are applied using the projection method of Olsson [29]. We present the differencing algorithm in detail, and indicate precisely how boundary conditions are applied.

This paper is organized as follows: In Sec. II we motivate our approach and review the overlapping grid method. We recall the concept of conserved energy for a first order symmetrizable hyperbolic system in Sec. III and provide an energy preserving discretization. In Sec. IV we analyze the axisymmetric wave equation around a Minkowski background as an introduction to our numerical methods. The analysis is then repeated for the black hole background case in Sec. V. The excision of a boosted black hole with the overlapping grid method is described in Sec. VI. The numerical experiments, along with several convergence tests, are included in Sec. VII.

II. OVERVIEW

Our primary goal is to obtain a numerical algorithm for excision with moving black holes that is stable and convergent (in the limit that the mesh spacing goes to zero). These desired properties for the discrete system closely mirror the continuum properties of well-posed initial boundary value problems (IBVPs): the existence of a unique solution that depends continuously on the initial and boundary data. Furthermore, we believe that we will not obtain long-term convergent discrete solutions *unless* the underlying continuum problem is also

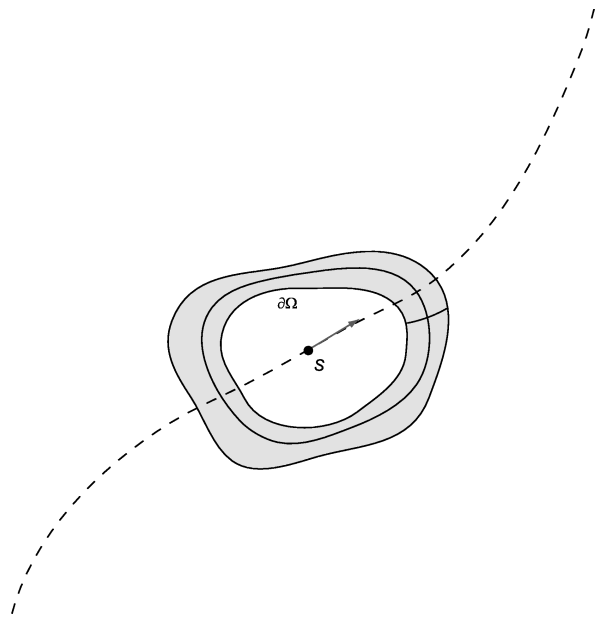


FIG. 1: A singularity S surrounded by an event horizon $\partial\Omega$ is moving with respect to the base coordinate system. A coordinate patch (shaded region) adapted to $\partial\Omega$ follows the motion of the singularity. With respect to this patch, $\partial\Omega$ is a purely outflow boundary and requires no boundary conditions. The base system terminates somewhere inside the shaded region and it gets boundary data from the moving patch. Similarly, the data at the outer boundary of the moving patch is taken from the base system.

well-posed. Unfortunately there are few mathematical results concerning the well-posedness of general classes of equations. The energy method, however, can be used with symmetric hyperbolic IBVPs, and gives sufficient conditions for well-posedness.

When a black hole moves with respect to some coordinate system, the inner excision boundary must also move. We use multiple coordinate patches, such that every boundary is fixed with respect to at least one coordinate system. Coordinate transformations relate the coordinate systems, and become time dependent when the hole moves. The movement of the inner boundary is also expressed by these time-dependent coordinate transformations. These ideas are illustrated in Fig. 1. In our axially symmetric model problem of a scalar field on a boosted Schwarzschild spacetime, the computational frame is covered with cylindrical coordinates, while a second patch of spherical coordinates is co-moving with the black hole. (In these coordinates the event horizon is always located at $r = 2M$ while the time coordinate is taken from the cylindrical patch so that data on all grids are simultaneous.) The inner boundary of the spherical grid, located at or within the event horizon, is a simple outflow boundary, and requires no boundary condition. The cylindrical domain has an inner boundary somewhere near the black hole, whether inside or out-

side of the horizon is immaterial, as long as it is covered by the spherical coordinate patch. An exchange of information between the two coordinate patches is required to provide boundary conditions at the inner cylindrical boundary and the outer spherical boundary.

On each grid the discrete system is constructed using the energy method [27]. We define an energy for the semi-discrete system and, using difference operators that satisfy summation by parts, we obtain a discrete energy estimate [13]. Well-posed boundary conditions can then be identified by controlling the boundary terms of the discrete energy estimate. The conditions are discretized using Olsson's projection method [29]. In particular, the symmetry axis ($\rho = 0$ in canonical cylindrical coordinates) is included in the discrete energy estimate [30], allowing us to naturally obtain a stable discretization for axisymmetric systems.

We implement our excision algorithm using overlapping grids, also known as composite mesh difference method [27, 31, 32]. The two grids are coupled by interpolation, which is done for all the components of the fields being evolved. If the system is hyperbolic this means that one is actually over specifying the problem. However, as it is pointed out in Sec. 13.4 of [27] and as it is confirmed by our experiments, this does not lead to a numerical instability. The fully discretized system is completed by integrating the semi-discrete equations with an appropriate method for ODEs; we choose third and fourth order Runge-Kutta, which does not spoil the energy estimate of the semi-discrete system [13]. Kreiss-Oliger dissipation [33] is added to the scheme, as some explicit dissipation is generally necessary for stability with overlapping grids [35]. Whereas the stability theory for overlapping grids for elliptic problems is well developed, there are very few results concerning hyperbolic systems. Starius presents a stability proof for overlapping grids in one dimension [31]. Finally, we note that Thornburg has also explored multiple grids in the context of numerical relativity with black hole excision [36].

The structure of the overlapping grids used in this work is illustrated in Fig. 6. The additional complication of the axis of symmetry is discussed below. For simplicity we choose the outer boundary to be of rectangular shape. The introduction of a smooth spherical outer boundary, along with another grid overlapping with the base cylindrical grid, is certainly possible and, we believe, likely to improve the absorbing character of the outer boundary when the incoming fields are set to zero.

III. THE WAVE EQUATION

To demonstrate our excision algorithm, we choose the evolution of a massless Klein-Gordon scalar field on an axisymmetric, boosted Schwarzschild background as a model problem. In this section we summarize basic definitions for linear, first order hyperbolic initial-boundary value problems [19, 27]. We employ the energy method

to identify well-posed boundary conditions. The discrete version of this method, based on difference operators satisfying the summation by parts rule [37], is then used to discretize the right hand side of the system and the boundary conditions on a single rectangular grid. (For an introduction to these methods in the context of numerical relativity see Refs. [13, 38, 39].) We then introduce the axisymmetric scalar field equations on a curved background, along with their semi-discrete approximation.

In this paper we adopt the Einstein summation convention and geometrized units ($G = c = 1$). Latin indices range over the spatial dimensions, and Greek indices label spacetime components.

A. Hyperbolic systems in first order form

Consider a linear, first order, hyperbolic IBVP in two spatial dimensions, consisting of a system of partial differential evolution equations, and initial and boundary data, of the form

$$\begin{aligned} \partial_t u &= A^i(t, \vec{x}) \partial_i u + B(t, \vec{x}) u \quad (t, \vec{x}) \in [0, T] \times \Omega(1) \\ u(0, \vec{x}) &= f(\vec{x}) \quad \vec{x} \in \Omega \end{aligned} \quad (2)$$

$$Lu(t, \vec{x}) = g(t, \vec{x}) \quad (t, \vec{x}) \in [0, T] \times \partial\Omega, \quad (3)$$

where $i = 1, 2$, $u = u(t, \vec{x})$ and $f(\vec{x})$ are vector valued functions with m components, A^i and B are $m \times m$ matrices that depend on the spacetime coordinates but not on the solution u , and ∂_i stands for $\partial/\partial x^i$. The boundary of $\Omega \subset \mathbb{R}^2$ is assumed to be a simple smooth curve. The operator L and the data g that appear in the boundary condition (3) will be defined below in Eqs. (10–11).

1. Strong and symmetric hyperbolicity

System (1)–(3) is said to be *strongly* hyperbolic in $O \subset [0, T] \times \Omega$ if, at each point $(t_0, \vec{x}_0) \in O$, the matrix

$$\hat{P}(t_0, \vec{x}_0, \vec{\omega}) = A^j(t_0, \vec{x}_0) \omega_j, \quad (4)$$

with $\vec{\omega} \in \mathbb{R}^2$ and $|\vec{\omega}|^2 = \omega_1^2 + \omega_2^2 = 1$, can be brought into real diagonal form by a transformation $T(\vec{\omega})$, such that $T(\vec{\omega})$ and $T^{-1}(\vec{\omega})$ are uniformly bounded with respect to $\vec{\omega}$. The system is said to be *symmetric* or *symmetrizable* hyperbolic in O if, at each point $(t_0, \vec{x}_0) \in O$, there exists a smooth, symmetric positive definite matrix $H(t_0, \vec{x}_0)$, independent of $\vec{\omega}$, such that $HA^i = (HA^i)^T$ for $i = 1, 2$. The matrix H is usually called the *symmetrizer*. Clearly, a symmetric hyperbolic system is also strongly hyperbolic. Strong hyperbolicity is a necessary condition for well-posedness and consequently for the construction of stable numerical schemes.

2. Characteristic speeds

The *characteristic speeds* in the direction $\vec{n} = (n_1, n_2) \in \mathbb{R}^2$, with $n_1^2 + n_2^2 = 1$, at the point $(t_0, \vec{x}_0) \in$

$[0, T] \times \Omega$ are the eigenvalues of $A^n(t_0, \vec{x}_0) \equiv n_i A^i(t_0, \vec{x}_0)$. In Sec. VII we will show how the maximum value of the characteristic speeds in the region $[0, T] \times \Omega$ can be used to compute an upper bound for the ratio between the time step and the spatial mesh size.

3. Energy method

The specification of proper boundary conditions requires careful consideration in order to achieve a well-posed IBVP, and we use the energy method to identify appropriate boundary conditions [27, 40]. Here one defines the energy of the system at time t to be

$$E(t) = \|u(t, \cdot)\|_H^2 = \int_{\Omega} u^T(t, \vec{x}) H(t, \vec{x}) u(t, \vec{x}) d^2x, \quad (5)$$

where H is some positive definite $m \times m$ symmetric matrix and u^T denotes the transpose of u . To ensure continuous dependence of the solution on the initial and boundary data, the energy must be bounded in terms of appropriate norms of the data. To determine this bound one usually takes a time derivative of the energy (5), with the further assumptions that u is a smooth solution of (1) and that H is a symmetrizer. The energy estimate is then

$$\begin{aligned} \frac{d}{dt} E(t) &= \int_{\partial\Omega} u^T H A^n u d\sigma \quad (6) \\ &+ \int_{\Omega} u^T (\partial_t H + H B + (H B)^T - \partial_i (H A^i)) u d^2x, \end{aligned}$$

where Gauss' theorem was used to obtain the boundary term, and n_i is the outward unit normal to the boundary $\partial\Omega$. To control the growth of the energy of the solution, we naturally need to control both the boundary and volume integrals. We consider the boundary integral first.

The matrix HA^n is symmetric, and can be brought into diagonal form by an orthogonal transformation $Q(n)$,

$$Q^T(n) H A^n Q(n) = \Lambda = \text{diag}(\Lambda_+, -\Lambda_-, 0), \quad (7)$$

where $\Lambda_{\pm} > 0$ are positive definite diagonal matrices, the eigenvalues of which, in general, do not coincide with the characteristic speeds. This allows one to rewrite the integrand of the boundary integral in Eq. (6) by introducing the vector $w^{(n)} = (w^{(+\Lambda_+;n)}, w^{(-\Lambda_-;n)}, w^{(0;n)})^T = Q^T(n)u$ as the difference between two non-negative terms,

$$\begin{aligned} u^T H A^n u &= \quad (8) \\ w^{(+\Lambda_+;n)T} \Lambda_+ w^{(+\Lambda_+;n)} &- w^{(-\Lambda_-;n)T} \Lambda_- w^{(-\Lambda_-;n)}. \end{aligned}$$

The components of $w^{(n)}$ are the *characteristic variables* in the direction \vec{n} . In particular, the components of $w^{(+\Lambda_+;n)}$ are the *ingoing* characteristic variables, and the components of $w^{(-\Lambda_-;n)}$ are the *outgoing* characteristic variables. We see that prescribing homogeneous

boundary conditions ($w^{(+\Lambda_+;n)} = Sw^{(-\Lambda_-;n)}$), with S sufficiently small, i.e., $S^T \Lambda_+ S \leq \Lambda_-$, ensures that the boundary term will give a non-positive contribution to the energy estimate. The $S = 0$ case (no coupling) is of particular interest as it usually yields a good approximation for absorbing (Sommerfeld) boundary conditions.

The second term of the energy estimate (6), the volume integral, can be estimated by $2\alpha \|u(t, \cdot)\|_H^2$, where $\alpha = \frac{1}{2} \max_{(t, \bar{x})} \|\partial_t H + HB + (HB)^T - \partial_i(HA^i)\|$ is a constant that does not depend on the solution. Thus, for homogeneous boundary conditions we have

$$\frac{d}{dt} \|u(t, \cdot)\|_H^2 \leq 2\alpha \|u(t, \cdot)\|_H^2, \quad (9)$$

which implies that $\|u(t, \cdot)\|_H \leq \exp(\alpha t) \|f\|_H$. Similar energy estimates can be obtained for inhomogeneous boundary conditions [27, 40], i.e.,

$$w^{(+\Lambda_+;n)} = Sw^{(-\Lambda_-;n)} + g, \quad (10)$$

where g has to satisfy compatibility conditions with the initial data.

Boundary conditions of the form (10) are referred to as *maximally dissipative* boundary conditions [41]. From Eq. (10) we see that the operator L introduced in (3) has the form

$$L = P^{(+)} Q^T(n) - S P^{(-)} Q^T(n), \quad (11)$$

where $P^{(+)}(w^{(+)}, w^{(-)}, w^0)^T = (w^{(+)}, 0, 0)^T$ and $P^{(-)}(w^{(+)}, w^{(-)}, w^0)^T = (0, w^{(-)}, 0)^T$. Finally, it is important to recognize that if the matrix H is not a symmetrizer, as would be the case if H symmetrizes A^i but fails to be positive definite, then the boundary condition above will not, in general, lead to a well-posed problem, as one would likely end up specifying boundary data to the wrong quantities.

4. Strict stability

Discretizing the spatial derivatives in the right hand side of system (1), but leaving time continuous, leads to a system of ODEs called the *semi-discrete system*. If an initial value problem satisfies the estimate $\|u(t, \cdot)\|_H \leq K \exp(\alpha t) \|u(0, \cdot)\|_H$ at the continuum, it would be desirable to obtain a discretization such that a similar estimate holds at the discrete level. Following [27], we will say that a semi-discrete system is *strictly stable* if

$$\|u(t)\|_h \leq K_S e^{\alpha_S t} \|u(0)\|_h \quad (12)$$

where $\alpha_S \leq \alpha + \mathcal{O}(h)$ and $\|\cdot\|_h$ is a discrete energy consistent with the one of the continuum.

5. Conserved energy

Clearly, the requirement that HA^i be symmetric, does not uniquely determine the symmetrizer. For example,

if H is a symmetrizer, then fH with $f > 0$ is also a symmetrizer. In some circumstances, as for the scalar field considered here, it is possible to select a preferred symmetrizer which satisfies the additional requirement

$$\partial_t H + HB + (HB)^T - \partial_i(HA^i) = 0. \quad (13)$$

When this condition holds, the energy defined by that symmetrizer will be conserved. By this we mean that the change in energy of our system is solely due to the boundary term of (6), which can be controlled by using maximal dissipative boundary conditions (10). In particular, when homogeneous boundary conditions are used, or when no boundaries are present, the energy cannot increase.

6. Energy conserving schemes

Let us assume momentarily that there exists a symmetrizer for which Eq. (13) holds (the system admits a conserved energy), and that no boundaries are present. In the variable coefficient case (more precisely, if $\partial_j(HA^i) \neq 0$ for $i = j$), the naive discretization $\partial_t u = A^i D_i u + Bu$, where u now represents a vector valued grid function, although strictly stable when a second order accurate centered difference operator is used [29], does not conserve the discrete energy

$$E = (u, Hu)_h = h_1 h_2 \sum_{ij} u_{ij}^T H_{ij} u_{ij}, \quad (14)$$

where $H_{ij} = H(t, \bar{x}_{ij})$. Its time derivative gives

$$\frac{d}{dt} E(t) = (u, [HA^i, D_i]u)_h + (u, \partial_i(HA^i)u)_h \neq 0, \quad (15)$$

where we used the fact that $(v, D_i u)_h + (D_i v, u)_h = 0$. The lack of a Leibniz rule at the discrete level is only partly responsible for this. In general, even if this rule were satisfied, the discrete estimate would not vanish, $\frac{d}{dt} E = (u, (\partial_i(HA^i) - D_i(HA^i))u)_h \neq 0$. Any semi-discrete approximation that preserves the discrete energy (14) is an *energy conserving* scheme. Remarkably, whenever a system admits a conserved energy at the continuum it is always possible to construct an energy conserving scheme [13, 38, 39]. The following “1/2 + 1/2” splitting, for example,

$$\begin{aligned} \partial_t u &= \frac{1}{2} A^i D_i u + \frac{1}{2} H^{-1} D_i (HA^i u) \\ &+ \left(B - \frac{1}{2} H^{-1} \partial_i (HA^i) \right) u, \end{aligned} \quad (16)$$

ensures that the discrete energy (14) remains constant. Clearly, an energy conserving scheme is strictly stable, since $\alpha = \alpha_S = 0$. We note that, depending on the problem, there may be alternative, simpler discretizations than the “1/2 + 1/2” splitting which lead to the same energy estimate. Moreover, a discretization such as (16) is a consistent approximation of $\partial_t u = A^i \partial_i u + Bu$ whether or not condition (13) holds.

7. Rectangular grid

Consider a rectangular domain $\Omega = \{(x^1, x^2) | x_{\min}^1 \leq x^1 \leq x_{\max}^1, x_{\min}^2 \leq x^2 \leq x_{\max}^2\}$, with the grid points $\bar{x}_{ij} = (x_{\min}^1 + ih_1, x_{\min}^2 + jh_2)$, $i = 0, \dots, N_1$ and $j = 0, \dots, N_2$, and $h_k = (x_{\max}^k - x_{\min}^k)/N_k$, $k = 1, 2$. From the continuum analysis we expect that boundary data should be given to the incoming characteristic variables in the direction orthogonal to the boundary surface. In addition, at the corners the boundary data has to satisfy compatibility conditions. We now repeat the same analysis for the semi-discrete system in order to determine appropriate boundary conditions for the computational grid. In particular, we examine the application of boundary conditions at the corner points of the grid.

We define the following one dimensional scalar products between vector valued grid functions,

$$(u, v)_{h_1} = h_1 \sum_{i=0}^{N_1} u_i^T v_i \sigma_i, \quad (u, v)_{h_2} = h_2 \sum_{i=0}^{N_2} u_i^T v_i \sigma_i, \quad (17)$$

where $\sigma_i = \{1/2, 1, \dots, 1, 1/2\}$. The 2D scalar product is

$$(u, v)_h = h_1 h_2 \sum_{i=0}^{N_1} \sum_{j=0}^{N_2} u_{ij}^T v_{ij} \sigma_i \sigma_j. \quad (18)$$

To simplify the notation we introduce $D^{(i)} = D^{(x^i)}$. If we approximate ∂_1 with the second order centered difference operator $D_0^{(1)} u_{ij} = (u_{i+1,j} - u_{i-1,j})/(2h_1)$ in the interior ($1 \leq i \leq N_1 - 1$, $0 \leq j \leq N_2$) and with the first order one-sided difference operators $D_+^{(1)} u_{0j} = (u_{1,j} - u_{0,j})/h_1$, $D_-^{(1)} u_{N_1j} = (u_{N_1,j} - u_{N_1-1,j})/h_1$ at the $x^1 = \text{const.}$ boundary we have that

$$\begin{aligned} & (u, D^{(1)}v)_h + (D^{(1)}u, v)_h \\ &= h_2 \sum_{j=0}^{N_2} \left(h_1 \sum_{i=0}^{N_1} u_{ij} D^{(1)}v_{ij} \sigma_i + h_1 \sum_{i=0}^{N_1} D^{(1)}u_{ij} v_{ij} \sigma_i \right) \sigma_j \\ &= (u_{i \cdot}, v_{i \cdot})_{h_2} \Big|_{i=0}^{i=N_1}. \end{aligned} \quad (19)$$

Similarly, if $D^{(2)} = D_0^{(2)}$ in the interior and $D^{(2)} = D_{\pm}^{(2)}$ at the $x^2 = \text{const.}$ boundary, we have that

$$(u, D^{(2)}v)_h + (D^{(2)}u, v)_h = (u_{\cdot j}, v_{\cdot j})_{h_1} \Big|_{j=0}^{j=N_2}. \quad (20)$$

If these simple finite difference operators are used to approximate the spatial derivatives in, for example, (16), the time derivative of the discrete energy

$$E = (u, Hu)_h = h_1 h_2 \sum_{ij} u_{ij}^T H_{ij} u_{ij} \sigma_i \sigma_j, \quad (21)$$

gives

$$\begin{aligned} \frac{d}{dt} E &= (u_{i \cdot}, (HA^1 u)_{i \cdot})_{h_2} \Big|_{i=0}^{i=N_1} + (u_{\cdot j}, (HA^2 u)_{\cdot j})_{h_1} \Big|_{j=0}^{j=N_2} \\ &\quad + (u, (\partial_t H + HB + (HB)^T - \partial_i (HA^i))u)_h, \end{aligned} \quad (22)$$

where we have not assumed energy conservation.

According to the discrete energy estimate above, to control the energy growth due to the boundary term, one should give data to the incoming variables in the direction \vec{n} , orthogonal to the boundary in maximally dissipative form, as shown in Fig. 2. To define the unit normal at the corner of the grid we examine the contribution to the energy estimate due to the corner point itself [29]. We see that, for example, at $(i, j) = (N_1, N_2)$ we have

$$\begin{aligned} & \frac{h_2}{2} u_{N_1 N_2}^T (HA^1 u)_{N_1 N_2} + \frac{h_1}{2} u_{N_1 N_2}^T (HA^2 u)_{N_1 N_2} \\ &= \frac{|h|}{2} u_{N_1 N_2}^T (HA^n u)_{N_1 N_2}, \end{aligned} \quad (23)$$

where $|h| = \sqrt{h_1^2 + h_2^2}$ and $\vec{n} = (h_2, h_1)/|h|$ is the unit normal at (N_1, N_2) . Similar results hold at the other corners. In particular, this shows that for uniform grids ($h_1 = h_2$), data should be given in the 45° direction.

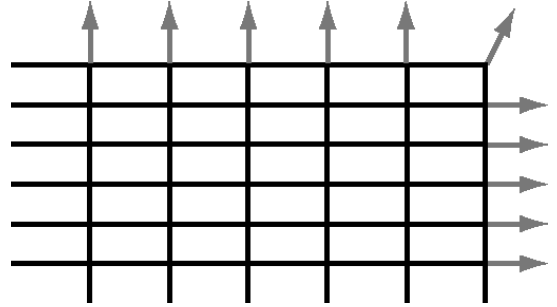


FIG. 2: The energy estimate for the semi-discrete initial-boundary value problem on domains with corners shows that, in order to control the growth due to the boundary term, boundary data must be given to the incoming modes with respect to the unit normal \vec{n} . At the corner, the unit normal depends on the mesh spacings h_1 and h_2 .

8. Olsson's boundary conditions

Let's assume that at the boundary there is one incoming, one outgoing, and one zero speed mode and that $\Lambda = \text{diag}(+\lambda_+, -\lambda_-, 0)$ with $\lambda_{\pm} > 0$. At each grid point belonging to the boundary, boundary conditions are implemented according to Olsson's prescription [29]. Namely, if $\vec{n} = (n_1, n_2)$ is the outward pointing unit normal, we carry out the following steps:

1. Compute $(W_{\text{old}}^{(+\lambda_+; n)}, W_{\text{old}}^{(-\lambda_-; n)}, W_{\text{old}}^{(0; n)})^T = Q(n)^T \Pi$, where Π is the discretized right hand side and $Q(n)$ is the orthogonal matrix that diagonalizes the boundary matrix HA^n , $Q(n)^T HA^n Q(n) = \Lambda$.
2. If the boundary condition at the continuum is $w^{(+\lambda_+; n)} = S w^{(-\lambda_-; n)} + g$, overwrite the ingoing

and outgoing modes according to

$$W_{\text{new}}^{(+\lambda_+;n)} = \frac{S}{1+S^2}(SW_{\text{old}}^{(+\lambda_+;n)} + W_{\text{old}}^{(-\lambda_-;n)}) + \frac{1}{1+S^2}\partial_t g$$

$$W_{\text{new}}^{(-\lambda_-;n)} = \frac{1}{1+S^2}(SW_{\text{old}}^{(+\lambda_+;n)} + W_{\text{old}}^{(-\lambda_-;n)}) - \frac{S}{1+S^2}\partial_t g$$

and leave the zero speed mode unchanged, $W_{\text{new}}^{(0;n)} = W_{\text{old}}^{(0;n)}$. This will ensure that $W_{\text{new}}^{(+\lambda_+;n)} = SW_{\text{new}}^{(-\lambda_-;n)} + \partial_t g$ and that the following linear combination of in- and outgoing modes remains unchanged, $SW_{\text{new}}^{(+\lambda_+;n)} + W_{\text{new}}^{(-\lambda_-;n)} = SW_{\text{old}}^{(+\lambda_+;n)} + W_{\text{old}}^{(-\lambda_-;n)}$. Note that unless $S = 0$, the outgoing mode will be modified. When the exact solution is known, the boundary data required to reproduce it are $g = g^{(+\lambda_+;n)} - Sg^{(-\lambda_-;n)}$, where $g^{(+\lambda_+;n)}$ and $g^{(-\lambda_-;n)}$ are ingoing and outgoing characteristic variables of the exact solution.

3. The new modified rhs is obtained by multiplying $(W_{\text{new}}^{(+\lambda_+;n)}, W_{\text{new}}^{(-\lambda_-;n)}, W_{\text{new}}^{(0;n)})^T$ by $Q(n)$.

9. Consistency at corners

Although giving data to the incoming variables at the corner in the direction \vec{n} controls the energy growth and therefore ensures numerical stability, to achieve consistency with the boundary conditions used at the two adjacent sides some extra care is required. Let us assume that the normals to the two sides defining the corner are \vec{n} and \vec{m} and that $\Lambda = \text{diag}(+\lambda_+, -\lambda_-, 0)$ with $\lambda_{\pm} > 0$, i.e., on each side there is one ingoing, one outgoing and one zero speed mode. We give data to the incoming variables at the sides according to

$$w_{\text{new}}^{(+\lambda_+;n)} = g^{(n)}, \quad (24)$$

$$w_{\text{new}}^{(+\lambda_+;m)} = g^{(m)}, \quad (25)$$

where, for simplicity, we have assumed no coupling to the outgoing fields. At the continuum these two conditions will be satisfied also at the corner. Let us assume that at the corner data is given in the direction \vec{p} . We must translate (24) and (25) in terms of characteristic variables in the direction \vec{p} . If $Q(r)$ denotes the orthogonal matrix defining the characteristic variables in the generic direction \vec{r} , $w^{(r)} = Q^T(r)u$, then we find that at the corner we must use $w^{(\lambda_+;p)} = SW^{(-\lambda_-;p)} + g^{(p)}$, with a non-trivial coupling

$$S = -\frac{[Q^T(m)Q(p)]_{13}[Q^T(n)Q(p)]_{12} - (n \leftrightarrow m)}{[Q^T(m)Q(p)]_{13}[Q^T(n)Q(p)]_{11} - (n \leftrightarrow m)}, \quad (26)$$

and boundary data

$$g^{(p)} = \frac{[Q^T(m)Q(p)]_{13}g^{(n)} - (n \leftrightarrow m)}{[Q^T(m)Q(p)]_{13}[Q^T(n)Q(p)]_{11} - (n \leftrightarrow m)}, \quad (27)$$

where $[Q]_{ij}$ denotes the ij matrix element of Q . The notation $(n \leftrightarrow m)$ indicates that the preceding term is

repeated with the exchange of the vectors m and n . In particular, if $g^{(n)}$ and $g^{(m)}$ vanish, then $g^{(p)}$ also vanishes. However, in general, the absence of coupling on the two adjacent sides is not consistent with a vanishing S at the corner, Eq. (26).

B. The massless scalar field on a curved background

1. The axially symmetric system

We now turn to the massless scalar field propagating on a curved background (M, g) . The equation of motion is the second order wave equation

$$\nabla_{\mu}\nabla^{\mu}\Phi = 0, \quad (28)$$

where ∇ denotes the covariant derivative associated with the Lorentz metric g . In terms of the tensor density $\gamma^{\mu\nu} = \sqrt{-g}g^{\mu\nu}$, the wave equation can be written

$$\partial_{\mu}(\gamma^{\mu\nu}\partial_{\nu}\Phi) = 0. \quad (29)$$

We introduce the auxiliary variables $T = \partial_t\Phi$ and $d_i = \partial_i\Phi$, and rewrite Eq. (29) in first order form,

$$\partial_t\Phi = T, \quad (30)$$

$$\partial_t T = -(\gamma^{ti}\partial_i T + \partial_i(\gamma^{it}T) + \partial_i(\gamma^{ij}d_j) + \partial_t\gamma^{tt}T + \partial_t\gamma^{tj}d_j)/\gamma^{tt}, \quad (31)$$

$$\partial_t d_i = \partial_i T. \quad (32)$$

The Φ component of a sufficiently smooth solution (Φ, T, d_i) of the first order system satisfies the second order wave equation provided that the constraints $C_i \equiv d_i - \partial_i\Phi = 0$ are satisfied. An attractive feature of this particular first order formulation is that the constraint variables propagate trivially, namely $\partial_t C_i = 0$ [13]. In particular, this ensures that any solution of (30–32) which satisfies the constraints initially, will satisfy them at later times, even in the presence of boundaries.

Since Φ does not appear in Eqs. (31–32), we will drop Eq. (30) from the system. The constraints are replaced by $C_{ij} \equiv \partial_{[i}d_{j]} = 0$, which also propagate trivially. Interestingly, if Eq. (32) and the constraints are discretized using difference operators satisfying $[D_i, D_j] = 0$, which is usually the case, then the time derivative of the discrete constraint variable $C_{ij} = D_{[i}d_{j]}$ will also vanish. In particular, for initial data such that $d_i = 0$, the discrete constraints will be identically satisfied during evolution.

To simplify the problem we assume that the background metric is axisymmetric, which implies that there exists a spacelike Killing field $\psi = \psi^{\mu}\partial_{\mu} = \partial_{\phi}$. We always use coordinate systems adapted to the Killing field, so that the metric components are independent of the ϕ coordinate and, in particular, $\partial_{\phi}\gamma^{\mu\nu} = 0$. Since we are only interested in axisymmetric solutions of the wave equation, i.e., solutions which do not depend on ϕ , the

variable d_ϕ can be eliminated from the system. Thus, the first order axisymmetric wave equation consists of Eq. (31) and (32), where the Latin indices now span only two dimensions, and one constraint.

2. Characteristic speeds

The characteristic speeds in an arbitrary direction \vec{n} , with $|\vec{n}| = 1$, are given by the eigenvalues of

$$A^n = A^i n_i = \begin{pmatrix} -2\gamma^{tn}/\gamma^{tt} & -\gamma^{nj}/\gamma^{tt} \\ n_i & 0 \end{pmatrix}. \quad (33)$$

These eigenvalues are $s_\pm = (\gamma^{tn} \pm \sqrt{(\gamma^{tn})^2 - \gamma^{tt}\gamma^{nn}})/(-\gamma^{tt}) = \beta^n \pm \alpha\sqrt{h^{nn}}$ and $s_0 = 0$, where α is the lapse function, β^i the shift vector, and h_{ij} is the induced 3-metric on the $t = \text{const.}$ slices in the ADM decomposition [42]. For the system to be hyperbolic it is essential that $(\gamma^{tn})^2 - \gamma^{tt}\gamma^{nn} = h^{nn} \geq 0$, which will be true as long as the $t = \text{const.}$ hypersurfaces are spacelike. We also need s_\pm to be bounded in the domain of interest, which will be the case in a cylindrical or spherical coordinate system (for $r \geq r_0 > 0$), provided that the solution does not depend on the azimuthal coordinate ϕ .

3. Symmetrizer, conserved energy, and characteristic variables

One can verify that

$$H(t, \vec{x}) = \eta(t, \vec{x}) \begin{pmatrix} -\gamma^{tt} & 0 \\ 0 & \gamma^{ij} \end{pmatrix} \quad (34)$$

is the most general symmetric matrix that satisfies $HA^i = (HA^i)^T$. When positive definite, which will be the case if and only if ∂_t is timelike and $\eta > 0$, it represents the most general symmetrizer of system (31–32). If we use a coordinate system adapted to the timelike Killing field $k = \partial_t$, the components of $\gamma^{\mu\nu}$ will be time independent. In this case the symmetrizer

$$H = \begin{pmatrix} -\gamma^{tt} & 0 \\ 0 & \gamma^{ij} \end{pmatrix} \quad (35)$$

satisfies Eq. (13) and gives rise to a conserved energy.

The boosting of the black hole will be performed by a Lorentz transformation. The time coordinate of the boosted frame will no longer be adapted to the timelike Killing field. In this case the time derivative of

$$E = \int_{\Omega} (-\gamma^{tt}T^2 + \gamma^{ij}d_i d_j) d^2x \quad (36)$$

is given by

$$\begin{aligned} \frac{d}{dt}E &= 2 \int_{\partial\Omega} (T\gamma^{ti}T + T\gamma^{ij}d_j) n_i d\sigma \\ &+ \int_{\Omega} (T\partial_t\gamma^{tt}T + 2T\partial_t\gamma^{tj}d_j + d_i\partial_t\gamma^{ij}d_j) d^2x \end{aligned} \quad (37)$$

We assume that in a neighborhood of the outer boundary ∂_t is timelike. The integrand of the surface term can be written as

$$2(T\gamma^{ti}T + T\gamma^{ij}d_j)n_i = \lambda_+ w^{(+\lambda_+;n)^2} - \lambda_- w^{(-\lambda_-;n)^2} \quad (38)$$

where $\lambda_\pm = \gamma^n \pm \gamma^{tn}$ and

$$w^{(\pm\lambda_\pm;n)} = \pm \frac{\sqrt{1 \pm \hat{\gamma}^{tn}}}{\sqrt{2}} T + \frac{1}{\sqrt{2}} \frac{\hat{\gamma}^{in} d_i}{\sqrt{1 \pm \hat{\gamma}^{tn}}} \quad (39)$$

$$w^{(0;n)} = \gamma_\perp^i d_i \quad (40)$$

are the orthonormal characteristic variables of HA^n . To simplify the notation we have introduced the quantities $\gamma^n = \sqrt{\delta_{\mu\nu}\gamma^{\mu n}\gamma^{\nu n}}$, $\hat{\gamma}^{\mu n} = \gamma^{\mu n}/\gamma^n$ and γ_\perp^i . The latter satisfies $\delta_{ij}\gamma_\perp^i\gamma_\perp^j = 1$ and $\delta_{ij}\gamma_\perp^i\gamma^{jn} = 0$. To express the primitive variables in terms of the characteristic variables we invert Eqs. (39)–(40),

$$T = \frac{\sqrt{1 + \hat{\gamma}^{tn}}}{\sqrt{2}} w^{(+\lambda_+;n)} - \frac{\sqrt{1 - \hat{\gamma}^{tn}}}{\sqrt{2}} w^{(-\lambda_-;n)} \quad (41)$$

$$d_i = \frac{\hat{\gamma}^{in}}{\sqrt{2}} \left(\frac{w^{(+\lambda_+;n)}}{\sqrt{1 + \hat{\gamma}^{tn}}} + \frac{w^{(-\lambda_-;n)}}{\sqrt{1 - \hat{\gamma}^{tn}}} \right) + \gamma_\perp^i w^{(0;n)} \quad (42)$$

Equations (39)–(42) will be used in the boundary conditions.

4. Discretization

Even when there is no conserved energy, it may be desirable to discretize the right hand side of (31) and (32) in a manner that satisfies the optimal estimate (22), such as (16) or other alternatives, where the symmetrizer H is given by (35).

The discretization of the wave equation according to (16) leads to

$$\begin{aligned} \partial_t T &= - \left(\gamma^{ti} D_i T + D_i (\gamma^{it} T) + \frac{1}{2} D_i (\gamma^{ij} d_j) + \right. \\ &\quad \left. + \frac{1}{2} \gamma^{ij} D_i d_j + \frac{1}{2} \partial_i \gamma^{ij} d_j + \partial_t \gamma^{tt} T + \partial_t \gamma^{ti} d_i \right) / \gamma^{tt}, \\ \partial_t d_i &= \frac{1}{2} D_i T + \frac{1}{2} ({}^3\gamma^{-1})_{ik} D_j (\gamma^{kj} T) - \frac{1}{2} ({}^3\gamma^{-1})_{ik} \partial_j \gamma^{kj} T, \end{aligned}$$

where ${}^3\gamma^{-1}$ denotes the inverse of γ^{ij} .

Alternatively, one can simply replace the partial derivative ∂_i in Eq. (31) and (32) with the finite difference operator D_i satisfying (19) and (20) and obtain the semi-discrete system

$$\begin{aligned} \partial_t T &= - (\gamma^{ti} D_i T + D_i (\gamma^{it} T) + D_i (\gamma^{ij} d_j) + \\ &\quad + \partial_t \gamma^{tt} T + \partial_t \gamma^{tj} d_j) / \gamma^{tt}, \end{aligned} \quad (43)$$

$$\partial_t d_i = D_i T. \quad (44)$$

which also satisfies the estimate (22). It is this discretization that will be used throughout this work, even in the boosted black hole case ($\partial_t \gamma^{\mu\nu} \neq 0$), where the energy (36) is not conserved. We analyze the discretization at the axis of symmetry in the next sections.

IV. MINKOWSKI BACKGROUND

The energy method for constructing stable finite difference schemes has, until recently, received little attention in numerical relativity. Thus we first present the wave equation in axisymmetric Minkowski space to demonstrate the method, before moving to the more complicated black hole configurations. In this section we give energy preserving discretizations for cylindrical and spherical coordinates. In particular, we will show how to discretize the system on the axis of symmetry in an energy conserving way. The next section examines discretizations for a Schwarzschild black hole in Kerr–Schild spherical coordinates.

A. Cylindrical coordinates

1. The system

In a Minkowski background in cylindrical coordinates, $\{t, \rho, z, \phi\}$, the second order axisymmetric wave equation has the form

$$\partial_t^2 \Phi = \frac{1}{\rho} \partial_\rho (\rho \partial_\rho \Phi) + \partial_z^2 \Phi. \quad (45)$$

We consider the first order formulation

$$\partial_t T = \frac{1}{\rho} \partial_\rho (\rho P) + \partial_z Z, \quad (46)$$

$$\partial_t P = \partial_\rho T, \quad (47)$$

$$\partial_t Z = \partial_z T, \quad (48)$$

where $T = \partial_t \Phi$, $P = \partial_\rho \Phi$ and $Z = \partial_z \Phi$ are functions of $(t, \rho, z) \in [0, T] \times [0, \rho_{\max}] \times [z_{\min}, z_{\max}]$.

2. Regularity conditions at the axis $\rho = 0$

Smoothness at the $\rho = 0$ axis requires that the odd ρ -derivatives of the scalar field vanish on the axis, namely $\partial_\rho^{2n-1} \Phi(t, \rho, z)|_{\rho=0} = 0$ for $n = 1, 2, \dots$. This implies that the following conditions for the auxiliary variables T , P , and Z , have to hold during evolution

$$P|_{\rho=0} = \partial_\rho^{2n} P|_{\rho=0} = 0 \quad \text{for } n = 1, 2, \dots \quad (49)$$

$$\partial_\rho^{2n-1} T|_{\rho=0} = \partial_\rho^{2n-1} Z|_{\rho=0} = 0 \quad \text{for } n = 1, 2, \dots \quad (50)$$

If the initial data satisfies (49) and (50), and the prescription $P(t, 0, z) = 0$ is used as a boundary condition at $\rho = 0$, then the above conditions will hold at later times.

3. The boundary conditions

Since in this coordinate system ∂_t is a Killing field, the energy (36) is conserved. The time derivative of

$$E = \int_{z_{\min}}^{z_{\max}} \int_0^{\rho_{\max}} (T^2 + P^2 + Z^2) \rho d\rho dz \quad (51)$$

gives only boundary terms which can be controlled by giving appropriate boundary data

$$\begin{aligned} \frac{d}{dt} E &= 2 \int_{z_{\min}}^{z_{\max}} T(t, \rho_{\max}, z) R(t, \rho_{\max}, z) \rho_{\max} dz \\ &+ 2 \int_0^{\rho_{\max}} [T(t, \rho, z) Z(t, \rho, z)]_{z=z_{\min}}^{z=z_{\max}} \rho d\rho. \end{aligned} \quad (52)$$

4. Energy conserving discretization

The discretization of the right hand side of Eq. (46) at the $\rho = 0$ axis deserves special attention. As a consequence of the regularity conditions we have that

$$\lim_{\rho \rightarrow 0^+} \frac{1}{\rho} \partial_\rho (\rho P) = 2 \partial_\rho P|_{\rho=0}. \quad (53)$$

and therefore no infinities appear on the right hand side.

This suggests considering the semi-discrete approximation [30]

$$\partial_t T_{ij} = \begin{cases} 2D_+^{(\rho)} P_{0j} + D^{(z)} Z_{0j}, & i = 0 \\ \frac{1}{\rho_i} D^{(\rho)} (\rho P)_{ij} + D^{(z)} Z_{ij}, & i \geq 1 \end{cases} \quad (54)$$

$$\partial_t P_{ij} = D^{(\rho)} T_{ij}, \quad i \geq 1 \quad (55)$$

$$\partial_t Z_{ij} = D^{(z)} T_{ij}, \quad i \geq 0, \quad (56)$$

where $\rho_i = i \Delta \rho$ and $z_j = z_{\min} + j \Delta z$, with $N_\rho \Delta \rho = \rho_{\max}$ and $N_z \Delta z = z_{\max} - z_{\min}$. The difference operators $D^{(\rho)}$ and $D^{(z)}$ are second order accurate centered difference operators where their computation does not involve points which do not belong to the grid, and are first order accurate one sided difference operators otherwise. The regularity condition, $P_{0j} = 0$ for $j = 0, \dots, N_z$, is enforced for all t , and Eq. (49) ensures that $D_+^{(\rho)} P_{0j}$ is, in fact, a second order approximation. A solution of (54, 55, 56) conserves the discrete energy

$$\begin{aligned} E &= \sum_{j=0}^{N_z} \left[\sum_{i=1}^{N_\rho} (T_{ij}^2 + P_{ij}^2 + Z_{ij}^2) \rho_i \sigma_i \Delta \rho \right. \\ &\quad \left. + \frac{1}{4} (T_{0j}^2 + Z_{0j}^2) \Delta \rho^2 \right] \sigma_j \Delta z, \end{aligned} \quad (57)$$

which is consistent with the continuum expression (51). More precisely, using the fact that $\partial_t T_{0j} = \frac{2}{\Delta \rho} P_{1j} + D^{(z)} Z_{0j}$ and the basic properties of the finite difference

operators, one can see that the following estimate

$$\begin{aligned} \frac{d}{dt}E &= 2 \sum_{j=0}^{N_z} T_{N_{\rho}j} \rho_{N_{\rho}} P_{N_{\rho}j} \sigma_j \Delta z \\ &+ 2 \sum_{i=1}^{N_{\rho}} (T_{iN_z} Z_{iN_z} - T_{i0} Z_{i0}) \rho_i \sigma_i \Delta \rho \\ &+ \frac{1}{2} (T_{0N_z} Z_{0N_z} - T_{00} Z_{00}) \Delta \rho^2 \end{aligned} \quad (58)$$

holds, consistently with the continuum limit (52).

As it is pointed out in Section 12.7 of [27], one order less accuracy at the boundary is allowed, in the sense that it does not affect the overall accuracy of the scheme, provided that the physical boundary conditions are approximated to the same order as the differential operators at the inner points.

5. Discrete boundary conditions

By inspecting the boundary terms of the discrete energy estimate (58), we can readily see how the boundary data should be given at each boundary grid point ($j = 0$, $j = N_z$, and $i = N_{\rho}$). In the case of a uniform grid ($\Delta \rho = \Delta z$), in order to control the energy growth boundary data should be given in maximally dissipative form in the directions shown in Fig. 3.

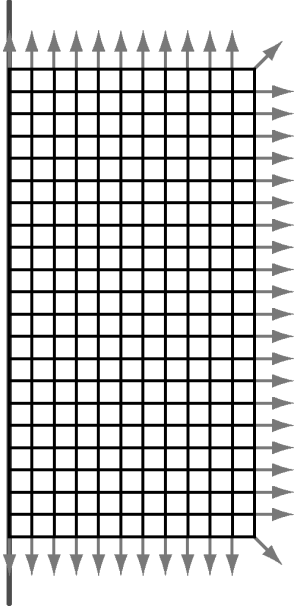


FIG. 3: This figure shows how the unit normal at the boundary grid points should be chosen. We note that at the corners which lie on the axis of symmetry we must apply both the regularity and the boundary conditions.

The presence of lower order terms in (57), in addition to ensuring that the discrete energy is positive definite

on the axis, indicates how to specify boundary data at the corner grid points that lie on the axis.

B. Spherical coordinates

In this section we discretize the wave equation in Minkowski space with spherical coordinates $\{t, r, \theta, \phi\}$.

1. The system

The second order axisymmetric wave equation on a flat background in spherical coordinates

$$\partial_t^2 \Phi = \frac{1}{r^2} \partial_r (r^2 \partial_r \Phi) + \frac{1}{r^2 \sin \theta} \partial_\theta (\sin \theta \partial_\theta \Phi), \quad (59)$$

is written in first order form as

$$\partial_t T = \frac{1}{r^2} \partial_r (r^2 R) + \frac{1}{r^2 \sin \theta} \partial_\theta (\sin \theta \Theta) \quad (60)$$

$$\partial_t R = \partial_r T \quad (61)$$

$$\partial_t \Theta = \partial_\theta T, \quad (62)$$

where $T = \partial_t \Phi$, $R = \partial_r \Phi$ and $\Theta = \partial_\theta \Phi$ are functions of $(t, r, \theta) \in [0, T] \times [r_{\min}, r_{\max}] \times [0, \pi]$.

2. Regularity conditions on the axis $\theta = 0$ and $\theta = \pi$

Smoothness requires that the odd θ -derivatives of the scalar field vanish on the axis of symmetry, namely at $\theta = 0$ and $\theta = \pi$. This implies that

$$\Theta|_{\theta=0,\pi} = \partial_\theta^{2n} \Theta|_{\theta=0,\pi} = 0 \quad n = 1, 2, \dots \quad (63)$$

$$\partial_\theta^{2n-1} T|_{\theta=0,\pi} = \partial_\theta^{2n-1} R|_{\theta=0,\pi} = 0 \quad n = 1, 2, \dots \quad (64)$$

As in the cylindrical case, it is possible to show that if the initial data satisfy (63) and (64) and the boundary conditions $\Theta|_{\theta=0,\pi} = 0$ are used during evolution, then the above regularity conditions will continue to hold.

3. Boundary conditions

Since we are interested in a domain of the form $\Omega = \{(r, \theta) \in \mathbb{R}^2 | r_{\min} \leq r \leq r_{\max}, 0 \leq \theta \leq \pi\}$, where $r_{\min} > 0$, the characteristic speeds are bounded by $\max\{1, r_{\min}^{-1}\}$. The conserved energy is

$$E = \int_{r_{\min}}^{r_{\max}} \int_0^\pi \left(T^2 + R^2 + \frac{\Theta^2}{r^2} \right) r^2 \sin \theta d\theta dr, \quad (65)$$

and its time derivative is given by

$$\frac{d}{dt}E = 2 \int_0^\pi r^2 RT|_{r=r_{\min}}^{r=r_{\max}} \sin \theta d\theta. \quad (66)$$

At $r = r_{\max}$ and $r = r_{\min}$ boundary data must be given to the incoming modes.

4. Energy conserving discretization

As a consequence of the regularity conditions on the axis of symmetry, we have that

$$\lim_{\theta \rightarrow m\pi} \frac{1}{\sin \theta} \partial_\theta (\sin \theta \Theta) = 2 \partial_\theta \Theta|_{\theta=m\pi}, \quad m = 0, 1. \quad (67)$$

$$\partial_t T_{ij} = \begin{cases} \frac{1}{r_i^2} D^{(r)}(r^2 R)_{ij} + \frac{2}{r_i^2} D_\pm^{(\theta)} \Theta_{ij} & j = 0, N_\theta \\ \frac{1}{r_i^2} D^{(r)}(r^2 R)_{ij} + \frac{1}{r_i^2 \sin \theta_j} D_0^{(\theta)} (\sin \theta \Theta)_{ij} & j = 1, \dots, N_\theta - 1 \end{cases} \quad (68)$$

$$\partial_t R_{ij} = D^{(r)} T_{ij}, \quad (69)$$

$$\partial_t \Theta_{ij} = D^{(\theta)} T_{ij}, \quad (70)$$

where $r_i = r_{\min} + i\Delta r$ and $\theta_j = j\Delta\theta$, with $N_r \Delta r = r_{\max} - r_{\min}$ and $N_\theta \Delta\theta = \pi$. The condition $\Theta_{i0} = \Theta_{iN_\theta} = 0$ on the axis is enforced at all times. The following discrete energy

$$\begin{aligned} E &= \sum_{i=0}^{N_r} \sum_{j=1}^{N_\theta-1} \left(T_{ij}^2 + R_{ij}^2 + \frac{\Theta_{ij}^2}{r_i^2} \right) r_i^2 \sin \theta_j \sigma_i \Delta\theta \Delta r \\ &+ \frac{1}{2} \sum_{i=0}^{N_r} (T_{i0}^2 + R_{i0}^2) r_i^2 \sigma_i \sin \Delta\theta \frac{\Delta\theta}{2} \Delta r \\ &+ \frac{1}{2} \sum_{i=0}^{N_r} (T_{iN_\theta}^2 + R_{iN_\theta}^2) r_i^2 \sigma_i \sin \Delta\theta \frac{\Delta\theta}{2} \Delta r, \end{aligned} \quad (71)$$

is conserved by the semi-discrete system. Its time derivative

$$\begin{aligned} \frac{d}{dt} E &= 2 \sum_{j=1}^{N_\theta-1} (T_{ij} R_{ij} r_i^2)|_{i=0}^{i=N_r} \sin \theta_j \Delta\theta \\ &+ (T_{i0} R_{i0} r_i^2)|_{i=0}^{i=N_r} \sin \Delta\theta \frac{\Delta\theta}{2} \\ &+ (T_{iN_\theta} R_{iN_\theta} r_i^2)|_{i=0}^{i=N_r} \sin \Delta\theta \frac{\Delta\theta}{2}, \end{aligned} \quad (72)$$

gives only boundary terms consistently with the continuum estimate (66).

5. Discrete boundary conditions

The choice of unit normal at the boundary grid points ($i = 0$ and $i = N_r$) is illustrated in Fig. 4.

V. FIXED BLACK HOLE BACKGROUND

This section is a generalization of the results of the previous section to the case of a static black hole background. The background metric is Schwarzschild in

We discretize the right hand side of (60–62) as

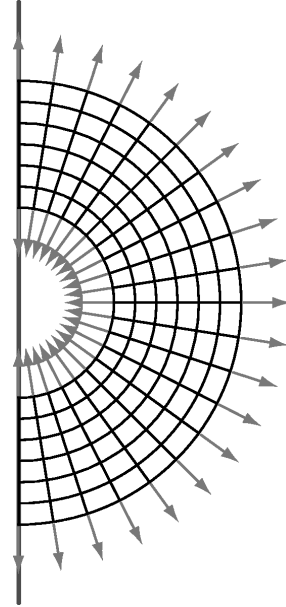


FIG. 4: According to the discrete energy estimate, boundary data should be given to the incoming variable in the direction indicated in the figure.

Kerr–Schild coordinates [43]. The Cartesian components of the background metric can be written as

$$g_{\mu\nu} = \eta_{\mu\nu} + \frac{2M}{r} \ell_\mu \ell_\nu, \quad (73)$$

where $\eta_{\mu\nu} = \text{diag}(-1, +1, +1, +1)$, $r^2 = x^2 + y^2 + z^2$ and $\ell_\mu = (1, \vec{x}/r)$. In these coordinates the determinant of the four-metric is $g = -1$.

The tensor density components $\gamma^{\mu\nu}$, which are needed to write down the 3D wave equation in first order form, are given by

$$\gamma^{\mu\nu} = \eta^{\mu\nu} - \frac{2M}{r} \ell^\mu \ell^\nu, \quad (74)$$

where $\ell^\mu = \eta^{\mu\nu}\ell_\nu = (-1, \vec{x}/r)$.

As we do not wish to consider cylindrical excision in this paper, we analyze here only the spherical coordinate case.

A. Spherical coordinates

1. The system

In spherical Kerr–Schild coordinates the components of $\gamma^{\mu\nu}$ on a Schwarzschild background are

$$\gamma^{\mu\nu} = r^2 \sin \theta \left(\eta^{\mu\nu} - \frac{2M}{r} l^\mu l^\nu \right), \quad (75)$$

$$\eta^{\mu\nu} = \text{diag} \left\{ -1, +1, +\frac{1}{r^2}, +\frac{1}{r^2 \sin^2 \theta} \right\},$$

$$\ell^\mu = (-1, +1, 0, 0).$$

The first order axisymmetric wave equation is

$$\partial_t T = \frac{2M}{r^+} \partial_r T + \frac{2M}{rr^+} \partial_r (rT) + \frac{1}{rr^+} \partial_r (rr^- R) \quad (76)$$

$$+ \frac{1}{rr^+ \sin \theta} \partial_\theta (\sin \theta \Theta)$$

$$\partial_t R = \partial_r T \quad (77)$$

$$\partial_t \Theta = \partial_\theta T, \quad (78)$$

where $r^\pm = r \pm 2M$, $T = \partial_t \Phi$, $R = \partial_r \Phi$ and $\Theta = \partial_\theta \Phi$. In the region of interest, $\Omega = \{(r, \theta) \in \mathbb{R}^2 | 2M \leq r \leq r_{\max}, 0 \leq \theta \leq \pi\}$, with $M > 0$, the characteristic speeds are bounded.

2. Regularity conditions on the axis $\theta = 0$ and $\theta = \pi$

Smoothness requires that the odd θ -derivatives of the scalar field vanish on the axis of symmetry. This implies

that

$$\Theta|_{\theta=0, \pi} = \partial_\theta^{2n} \Theta|_{\theta=0, \pi} = 0 \quad n = 1, 2, \dots \quad (79)$$

$$\partial_\theta^{2n-1} T|_{\theta=0, \pi} = \partial_\theta^{2n-1} R|_{\theta=0, \pi} = 0 \quad n = 1, 2, \dots \quad (80)$$

3. The boundary conditions

A symmetrizer which gives rise to a conserved energy is given by

$$H = \text{diag}\{rr^+ \sin \theta, rr^- \sin \theta, \sin \theta\}, \quad (81)$$

which is positive definite for $0 < \theta < \pi$ and $r > 2M$. Inside the event horizon, $r < 2M$, the vector field ∂_t becomes spacelike and the system is only strongly hyperbolic.

The time derivative of the energy

$$E = \int_{2M}^{r_{\max}} \int_0^\pi (rr^+ T^2 + rr^- R^2 + \Theta^2) \sin \theta d\theta dr, \quad (82)$$

gives only boundary terms

$$\frac{d}{dt} E = 2 \int_0^\pi (2MrT^2 + rr^- TR) \Big|_{r=2M}^{r=r_{\max}} \sin \theta d\theta \quad (83)$$

In addition to the regularity condition $\Theta = 0$ at the axis, the problem requires boundary data at $r = r_{\max}$.

4. Energy conserving discretization

We discretize the right hand side of (76–78) as

$$\partial_t T_{ij} = \begin{cases} \frac{2M}{r_i^+} D^{(r)} T_{ij} + \frac{2M}{r_i r_i^+} D^{(r)} (rT)_{ij} + \frac{1}{r_i r_i^+} D^{(r)} (rr^- R)_{ij} + \frac{2}{r_i r_i^+} D_\pm^{(\theta)} \Theta_{ij} & j = 0, N_\theta \\ \frac{2M}{r_i^+} D^{(r)} T_{ij} + \frac{2M}{r_i r_i^+} D^{(r)} (rT)_{ij} + \frac{1}{r_i r_i^+} D^{(r)} (rr^- R)_{ij} + \frac{1}{r_i r_i^+ \sin \theta_j} D_0^{(\theta)} (\sin \theta \Theta)_{ij} & j = 1, \dots, N_\theta - 1 \end{cases} \quad (84)$$

$$\partial_t R_{ij} = D^{(r)} T_{ij} \quad (85)$$

$$\partial_t \Theta_{ij} = D^{(\theta)} T_{ij}, \quad (86)$$

where $r_i = 2M + i\Delta r$ and $\theta_j = j\Delta\theta$, with $N_r \Delta r = r_{\max} - 2M$ and $N_\theta \Delta\theta = \pi$. The following discrete energy,

$$E = \sum_{i=0}^{N_r} \sum_{j=1}^{N_\theta-1} (r_i r_i^+ T_{ij}^2 + r_i r_i^- R_{ij}^2 + \Theta_{ij}^2) \sin \theta_j \sigma_i \Delta\theta \Delta r$$

$$+ \frac{1}{2} \sum_{i=0}^{N_r} (r_i r_i^+ T_{i0}^2 + r_i r_i^- R_{i0}^2) \sigma_i \sin \Delta\theta \frac{\Delta\theta}{2} \Delta r$$

$$+ \frac{1}{2} \sum_{i=0}^{N_r} (r_i r_i^+ T_{iN_\theta}^2 + r_i r_i^- R_{iN_\theta}^2) \sigma_i \sin \Delta\theta \frac{\Delta\theta}{2} \Delta r,$$

is conserved. Its time derivative is given by

$$\begin{aligned} \frac{d}{dt}E &= 2 \sum_{j=1}^{N_\theta-1} (2Mr_i T_{ij}^2 + r_i r_i^- T_{ij} R_{ij}) \Big|_{i=0}^{i=N_r} \sin \theta_j \Delta\theta \\ &+ (2Mr_i T_{i0}^2 + r_i r_i^- T_{i0} R_{i0}) \Big|_{i=0}^{i=N_r} \sin \Delta\theta \frac{\Delta\theta}{2} \\ &+ (2Mr_i T_{iN_\theta}^2 + r_i r_i^- T_{iN_\theta} R_{iN_\theta}) \Big|_{i=0}^{i=N_r} \sin \Delta\theta \frac{\Delta\theta}{2}. \end{aligned}$$

We point out that, since $\Theta_{i0} = \Theta_{iN_\theta} = 0$, the discrete energy is positive definite on the axis. However, because $r_0^- = 0$, it does not control the growth of R_{0j} on the event horizon. Numerical experiments indicate that this does not cause any problems. Moreover, experiments do not suggest that placing r_{\min} within the horizon, where the equations are only strongly hyperbolic, leads to an unstable scheme.

5. Discrete boundary conditions

Data should be given to the incoming modes at $r = r_{\max}$ as in Fig. 4. Unlike the Minkowski case, no boundary conditions should be given when the inner boundary, $r = r_{\min}$, is at or within the event horizon.

VI. BOOSTED BLACK HOLE BACKGROUND

Finally, we consider the case in which the scalar field propagates on a boosted black hole background. To solve this problem we introduce two coordinate patches: one patch fixed to the outer boundaries and one patch comoving with the black hole, and fixed to the inner excision boundary. We choose cylindrical coordinates for the first coordinate patch, boosted with respect to the black hole such that the hole moves with velocity β along the symmetry axis in these coordinates. Spherical coordinates are used on the second patch. These coordinates are chosen by fixing the event horizon at a constant coordinate value ($r' = 2M$), and requiring that all data in both coordinate systems are simultaneous. By adapting these coordinates to the black hole horizon, we may excise the spherical grid at $r' = 2M$ for all values of the boost parameter. In this section we first write down the components of the 4-metric in a boosted Cartesian coordinate system, then discuss the two coordinate systems in some detail.

We recall that in a Cartesian coordinate system $\{t, x, y, z\}$, with respect to which the black hole is at rest, the metric components have the form given in (73). Under a Lorentz boost, i.e., in the new coordinates

$$\begin{aligned} \bar{t} &= \gamma(t - \beta z) \\ \bar{x} &= x \\ \bar{y} &= y \\ \bar{z} &= \gamma(z - \beta t), \end{aligned} \tag{87}$$

where $\gamma = (1 - \beta^2)^{-1/2}$, the components of the Kerr–Schild metric become

$$\begin{aligned} g_{\bar{\mu}\bar{\nu}} &= \eta_{\bar{\mu}\bar{\nu}} + \frac{2M}{r} \ell_{\bar{\mu}} \ell_{\bar{\nu}}, \\ \eta_{\bar{\mu}\bar{\nu}} &= \text{diag}\{-1, +1, +1, +1\}, \\ \ell_{\bar{\mu}} &= (\hat{r}, \bar{x}, \bar{y}, \hat{z})/r, \end{aligned}$$

where $\hat{r} = \gamma(r + \beta z)$, $\hat{z} = \gamma(z + \beta r)$, $z = \gamma(\bar{z} + \beta \bar{t})$ and $r^2 = x^2 + y^2 + z^2 = \bar{x}^2 + \bar{y}^2 + \gamma^2(\bar{z} + \beta \bar{t})^2$. At time \bar{t} the singularity is located at $(\bar{x}, \bar{y}, \bar{z}) = (0, 0, -\beta \bar{t})$.

A. Boosted cylindrical coordinates

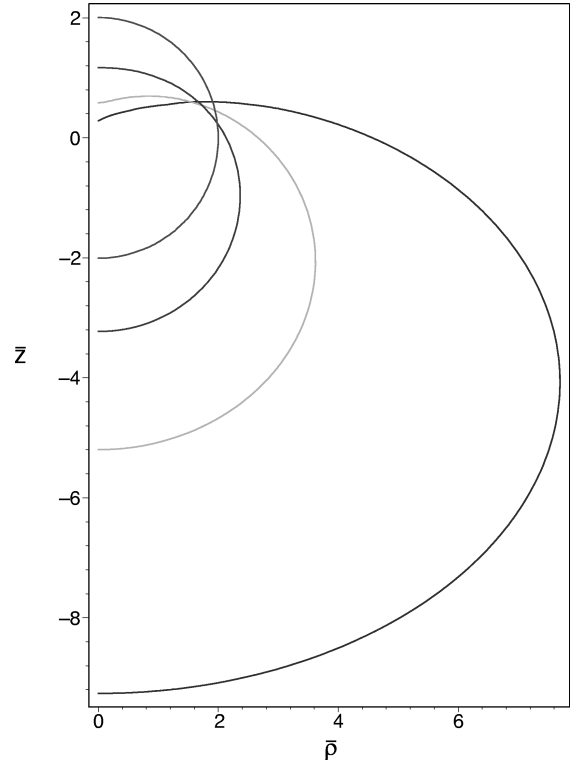


FIG. 5: The regions delimited by the curves are regions in which the system is not symmetrizable hyperbolic, but only strongly hyperbolic for $\beta = 0, -1/4, -1/2, -3/4$ (the black hole is located at $(\bar{\rho}, \bar{z}) = (0, 0)$ and moves in the $+\bar{z}$ direction). As the boost parameter β increases in magnitude there is a larger part of the cylindrical domain in which the system is only strongly hyperbolic.

We now choose cylindrical coordinates $\{\bar{t}, \bar{\rho}, \bar{z}, \bar{\phi}\}$, with $\bar{\rho} \cos \bar{\phi} = \bar{x}$ and $\bar{\rho} \sin \bar{\phi} = \bar{y}$, giving

$$\begin{aligned} g_{\bar{\mu}\bar{\nu}} &= \eta_{\bar{\mu}\bar{\nu}} + \frac{2M}{r} \ell_{\bar{\mu}} \ell_{\bar{\nu}}, \\ \eta_{\bar{\mu}\bar{\nu}} &= \text{diag}\{-1, +1, +1, +\bar{\rho}^2\}, \\ \ell_{\bar{\mu}} &= (\hat{r}, \bar{\rho}, \hat{z}, 0)/r \end{aligned}$$

and

$$\begin{aligned}\gamma^{\bar{\mu}\bar{\nu}} &= \bar{\rho} \left(\eta^{\bar{\mu}\bar{\nu}} - \frac{2M}{r} \ell^{\bar{\mu}} \ell^{\bar{\nu}} \right), \\ \eta^{\bar{\mu}\bar{\nu}} &= \text{diag}\{-1, +1, +1, +\frac{1}{\bar{\rho}^2}\}, \\ \ell^{\bar{\mu}} &= (-\hat{r}, \bar{\rho}, \hat{z}, 0) / r,\end{aligned}\quad (88)$$

where $z = \gamma(\bar{z} + \beta\bar{t})$ and $r^2 = \bar{\rho}^2 + \gamma^2(\bar{z} + \beta\bar{t})^2$. Unfortunately, in these coordinates the wave equation has a rather unpleasant form: the components of $\gamma^{\bar{\mu}\bar{\nu}}$ have a non-trivial dependence on the three coordinates $\bar{\rho}$ and \bar{z} , and especially, \bar{t} .

The analytic expressions for the time derivatives of the $\gamma^{\bar{\mu}\bar{\nu}}$ components are needed. Using the fact that $\partial_{\bar{t}}r = \beta\gamma z/r$, $\partial_{\bar{t}}\hat{r} = \beta\gamma\hat{z}/r$ and $\partial_{\bar{t}}\hat{z} = \beta\gamma\hat{r}/r$ we get

$$\begin{aligned}\partial_{\bar{t}}\gamma^{\bar{t}\bar{t}} &= 2M\beta\gamma\bar{\rho}\hat{r}(3z\hat{r} - 2r\hat{z})/r^5, \\ \partial_{\bar{t}}\gamma^{\bar{t}\bar{\rho}} &= 2M\beta\gamma\bar{\rho}^2(r\hat{z} - 3z\hat{r})/r^5, \\ \partial_{\bar{t}}\gamma^{\bar{t}\bar{z}} &= 2M\beta\gamma\bar{\rho}(r\hat{z}^2 + r\hat{r}^2 - 3z\hat{r}\hat{z})/r^5.\end{aligned}\quad (89)$$

In this coordinate system our first order formulation has no conserved energy ($\partial_{\bar{t}}\gamma^{\bar{\mu}\bar{\nu}} \neq 0$). The region in which the system is symmetric hyperbolic is determined by the set of points in which $\partial_{\bar{t}}$ is timelike,

$$-g_{\bar{t}\bar{t}} = 1 - \frac{2M\hat{r}^2}{r^3} > 0. \quad (90)$$

Fig. 5 shows the regions of lack of symmetric hyperbolicity for different values of the boost parameter.

On the axis of symmetry ($\bar{\rho} = 0$) the equations need to be expressed in a form which avoids “0/0”. This can be done by taking the limit $\bar{\rho} \rightarrow 0$ in the equations. It is convenient to introduce the quantities

$$\tilde{\gamma}^{\bar{t}\bar{t}} = \frac{\gamma^{\bar{t}\bar{t}}}{\bar{\rho}}, \quad \tilde{\gamma}^{\bar{t}\bar{\rho}} = \frac{\gamma^{\bar{t}\bar{\rho}}}{\bar{\rho}^2}, \quad \tilde{\gamma}^{\bar{t}\bar{z}} = \frac{\gamma^{\bar{t}\bar{z}}}{\bar{\rho}},$$

$$\tilde{\gamma}^{\bar{\rho}\bar{\rho}} = \frac{\gamma^{\bar{\rho}\bar{\rho}}}{\bar{\rho}}, \quad \tilde{\gamma}^{\bar{\rho}\bar{z}} = \frac{\gamma^{\bar{\rho}\bar{z}}}{\bar{\rho}^2}, \quad \tilde{\gamma}^{\bar{z}\bar{z}} = \frac{\gamma^{\bar{z}\bar{z}}}{\bar{\rho}},$$

which have a finite limit for $\bar{\rho} \rightarrow 0$ (since the singularity is excised we can assume that $r \geq r_0 > 0$). The right hand side of (31) at $\bar{\rho} = 0$ becomes

$$\begin{aligned}\partial_{\bar{t}}\bar{T} &= \left(\tilde{\gamma}^{\bar{t}\bar{z}}\partial_{\bar{z}}\bar{T} + 2\tilde{\gamma}^{\bar{t}\bar{\rho}}\bar{T} + \partial_{\bar{z}}(\tilde{\gamma}^{\bar{t}\bar{z}}\bar{T}) + 2\tilde{\gamma}^{\bar{\rho}\bar{\rho}}\partial_{\bar{\rho}}\bar{P} + \right. \\ &\quad \left. + 2\tilde{\gamma}^{\bar{\rho}\bar{z}}\bar{Z} + \partial_{\bar{z}}(\tilde{\gamma}^{\bar{\rho}\bar{z}}\bar{Z}) + \partial_{\bar{t}}\tilde{\gamma}^{\bar{t}\bar{t}}\bar{T} + \partial_{\bar{t}}\tilde{\gamma}^{\bar{t}\bar{z}}\bar{Z} \right) / (-\tilde{\gamma}^{\bar{t}\bar{t}}).\end{aligned}$$

B. Co-moving spherical coordinate system

We introduce a spherical coordinate system $\{t', r', \theta', \phi'\}$ which is related to the unboosted Cartesian coordinates $\{t, x, y, z\}$, the coordinates in which the black hole is at rest, by

$$\begin{aligned}t' &= \bar{t} = \gamma(t - \beta z) \\ r' &= \sqrt{x^2 + y^2 + z^2} \\ \theta' &= \cos^{-1} \left(\frac{z}{\sqrt{x^2 + y^2 + z^2}} \right) \\ \phi' &= \tan^{-1} \left(\frac{y}{x} \right).\end{aligned}\quad (91)$$

We emphasize that (91) is not a Lorentz transformation. The coordinates are adapted to the event horizon in the sense that its location ($r' = 2M$) is time independent, and setting $t' = \bar{t}$ maintains simultaneity in the two coordinate systems. The metric components and the components of $\gamma^{\mu'\nu'}$ are more conveniently written in matrix form

$$\begin{aligned}g_{\mu'\nu'} &= \begin{pmatrix} \frac{1}{\gamma^2} \left(-1 + \frac{2M}{r'} \right) & \frac{1}{\gamma} \left(\frac{2M}{r'} - \beta \cos \theta' \left(1 - \frac{2M}{r'} \right) \right) & \frac{1}{\gamma} (r' - 2M) \beta \sin \theta' & 0 \\ \cdot & (1 + \beta \cos \theta') \left(1 - \beta \cos \theta' + \frac{2M}{r'} (1 + \beta \cos \theta') \right) & \beta \sin \theta' \left((r' - 2M) \beta \cos \theta' - 2M \right) & 0 \\ \cdot & \cdot & r' (r' - \beta^2 \sin^2 \theta' (r' - 2M)) & 0 \\ \cdot & \cdot & \cdot & r'^2 \sin^2 \theta' \end{pmatrix} \\ \gamma^{\mu'\nu'} &= \begin{pmatrix} -\frac{1}{\gamma} r' \sin \theta' (r' + 2M\gamma^2(1 + \beta \cos \theta')^2) & r' \sin \theta' (2M - \beta \cos \theta' (r' - 2M)) & \beta r' \sin^2 \theta' & 0 \\ \cdot & \frac{1}{\gamma} r' (r' - 2M) \sin \theta' & 0 & 0 \\ \cdot & \cdot & \frac{\sin \theta'}{\gamma} & 0 \\ \cdot & \cdot & \cdot & \frac{1}{\gamma \sin \theta'} \end{pmatrix}.\end{aligned}\quad (92)$$

We have symmetric hyperbolicity for $r' > 2M$ and $0 < \theta' < \pi$.

On the axis of symmetry ($\theta' = 0$ or $\theta' = \pi$) the equations need to be expressed in a form that avoids “0/0”. This can be done by taking the limit $\theta' \rightarrow \theta_0$, where

$\theta_0 = 0, \pi$ in the equations. If we introduce the quantities

$$\begin{aligned}\tilde{\gamma}^{t't'} &= \frac{\gamma^{t't'}}{\sin \theta'}, & \tilde{\gamma}^{t'r'} &= \frac{\gamma^{t'r'}}{\sin \theta'}, & \tilde{\gamma}^{t'\theta'} &= \frac{\gamma^{t'\theta'}}{\sin^2 \theta'}, \\ \tilde{\gamma}^{r'r'} &= \frac{\gamma^{r'r'}}{\sin \theta'}, & \tilde{\gamma}^{\theta'\theta'} &= \frac{\gamma^{\theta'\theta'}}{\sin \theta'},\end{aligned}$$

which have a finite limit for $\sin \theta' \rightarrow 0$, then the right hand side of (31) on axis becomes

$$\begin{aligned}\partial_{t'} T' &= \left(\tilde{\gamma}^{t'r'} \partial_{r'} T' + \partial_{r'} (\tilde{\gamma}^{t'r'} T') \pm 2\tilde{\gamma}^{t'\theta'} T' \right. \\ &\quad \left. + \partial_{r'} (\tilde{\gamma}^{r'r'} R') + 2\tilde{\gamma}^{\theta'\theta'} \partial_{\theta'} \Theta' \right) / (-\tilde{\gamma}^{t't'}),\end{aligned}\quad (93)$$

where the components of $\tilde{\gamma}^{\mu'\nu'}$ are understood to be evaluated at $\theta' = 0, \pi$.

C. Overlapping grids

As mentioned in Section II, the method of overlapping grids gives a natural method for solving finite difference problems on multiple domains. For the boosted black hole, we use the cylindrical grid as our base grid and introduce the spherical grid adapted to the inner boundary (event horizon). The two grids overlap as shown in Fig. 6.

The spherical grid requires boundary data at $r = r_{\max}$, which does not constitute a physical boundary in this problem. Here the data is computed by interpolating the values of the field from the cylindrical grid. Similarly, the values of the fields at the grid points of the cylindrical grid near the excision region, which lack a neighboring point in a coordinate direction (these points are marked with a square in Fig. 6), are also updated via interpolation. In this work we used second order Lagrangian interpolation, which, for a scalar quantity, is given by

$$\begin{aligned}f_{\text{Int}}(x_i + a\Delta x, y_j + b\Delta y) &= (1-a)(1-b)f_{ij} \\ &+ (1-a)bf_{i,j+1} + a(1-b)f_{i+1,j} + abf_{i+1,j+1}\end{aligned}$$

where $0 \leq a, b < 1$. Higher-order interpolation stencils may also be used, though for the cases examined here, improvements in the resulting solutions are slight, resulting in no increase in the order of accuracy.

The boosted cylindrical and co-moving spherical coordinate systems are related by

$$\begin{aligned}\bar{t} &= t' \\ \bar{\rho} &= r' \sin \theta' \\ \bar{z} &= \gamma^{-1} r' \cos \theta' - \beta t' \\ \bar{\phi} &= \phi',\end{aligned}\quad (94)$$

and the inverse transformation

$$\begin{aligned}t' &= \bar{t} \\ r' &= \sqrt{\bar{\rho}^2 + \gamma^2(\bar{z} + \beta\bar{t})^2} \\ \theta' &= \tan^{-1} \left(\frac{\bar{\rho}}{\gamma(\bar{z} + \beta\bar{t})} \right) \\ \phi' &= \bar{\phi}.\end{aligned}\quad (95)$$

The evolved fields are not scalar quantities, but components of a 1-form. So, in addition to the coordinate transformation between the two coordinate systems, the communication of the values of the fields requires the use of the transformation law of 1-forms. In this case we have

$$\bar{T} = T' + \gamma\beta \cos \theta' R' - \gamma\beta \frac{\sin \theta'}{r'} \Theta' \quad (96)$$

$$\bar{P} = \sin \theta' R' + \frac{\cos \theta'}{r'} \Theta'$$

$$\bar{Z} = \gamma \cos \theta' R' - \gamma \frac{\sin \theta'}{r'} \Theta',$$

and

$$T' = \bar{T} - \beta \bar{Z} \quad (97)$$

$$R' = \sin \theta' \bar{P} + \frac{\cos \theta'}{\gamma} \bar{Z}$$

$$\Theta' = r' \cos \theta' \bar{P} - r' \frac{\sin \theta'}{\gamma} \bar{Z},$$

where $(\bar{T}, \bar{P}, \bar{Z})$ and (T', R', Θ') are the fields on the cylindrical and spherical grids, respectively.

1. Discretization on the axis

The discretization of the system in boosted cylindrical coordinates in the interior and at the outer boundary is done according to Eqs. (43)–(44) where the components $\gamma^{\mu\nu}$ are given in (88). On the axis of symmetry we use

$$\begin{aligned}\partial_{\bar{t}} \bar{T} &= \left(\tilde{\gamma}^{\bar{t}\bar{z}} D^{(\bar{z})} \bar{T} + 2\tilde{\gamma}^{\bar{t}\bar{\rho}} \bar{T} + D^{(\bar{z})} (\tilde{\gamma}^{\bar{t}\bar{z}} \bar{T}) + 2\tilde{\gamma}^{\bar{\rho}\bar{\rho}} D_{\pm}^{(\bar{\rho})} \bar{P} + \right. \\ &\quad \left. 2\tilde{\gamma}^{\bar{\rho}\bar{z}} \bar{Z} + D^{(\bar{z})} (\tilde{\gamma}^{\bar{z}\bar{z}} \bar{Z}) + \partial_{\bar{t}} \tilde{\gamma}^{\bar{t}\bar{t}} \bar{T} + \partial_{\bar{t}} \tilde{\gamma}^{\bar{t}\bar{z}} \bar{Z} \right) / (-\tilde{\gamma}^{\bar{t}\bar{t}}).\end{aligned}$$

Similarly, the discretization of the system in co-moving spherical coordinates in the interior and on the event horizon is done according to Eqs. (43)–(44), where the components of $\gamma^{\mu'\nu'}$ are given in (92). On the axis of symmetry ($\theta = 0$ and $\theta = \pi$) we use

$$\begin{aligned}\partial_{t'} T' &= \left(\tilde{\gamma}^{t'r'} D^{(r')} T' + D^{(r')} (\tilde{\gamma}^{t'r'} T') \pm 2\tilde{\gamma}^{t'\theta'} T' + \right. \\ &\quad \left. D^{(r')} (\tilde{\gamma}^{r'r'} R') + 2\tilde{\gamma}^{\theta'\theta'} D_{\pm}^{(\theta')} \Theta' \right) / (-\tilde{\gamma}^{t't'}).\end{aligned}$$

2. Boundary conditions

Boundary conditions in maximally dissipative form are given at the outer boundary of the cylindrical grid in the directions indicated in Fig. 6. In the boosted case, instead of overwriting the right hand side at the boundary according to Olsson's prescription, we overwrite the solution itself. The reason for doing so, is that it avoids the tedious task of computing time derivatives of the boundary data.

It is interesting to notice that the outer boundary of the cylindrical grid could become at some points purely inflow ($s_{\pm} > 0$) for very large values of β . (We exclude the case in which the black hole is outside the outer boundary.) At and near these inflow boundary points the system is only strongly hyperbolic and the energy method fails to give the correct boundary conditions. As it is pointed out in [34], applying maximally dissipative boundary conditions to strongly hyperbolic systems can lead to an ill posed IBVP. Where the boundary is purely inflow we give data to the two incoming fields. Our numerical experiments (Sec. VII) indicate that the scheme is stable.

3. Artificial dissipation

Whereas the single grid schemes do not require any artificial dissipation, it is known that overlapping grids require explicit dissipation for stability [35]. To the right hand side of the discretized system a term of the form [33]

$$Q_d u = -\sigma \left(h_1^3 (D_+^{(1)} D_-^{(1)})^2 + h_2^3 (D_+^{(2)} D_-^{(2)})^2 \right) u \quad (98)$$

is added. This dissipative operator is modified near the outer and inner boundary, as was done in [13]. Near and on the axis of symmetry dissipation is computed exploiting the regularity conditions of the fields. As this dissipation has a five-point stencil, we find that the long-term behavior of the code is improved in some cases by interpolating two points at all inter-grid boundaries.

4. Choice of Courant factor

The fully discrete system is obtained by integrating the semi-discrete system with third or fourth order Runge-Kutta. Whenever explicit finite difference schemes are used to approximate hyperbolic problems, the ratio between the time step size k and the mesh size $h = \min\{h_i\}$, the *Courant factor*, cannot be greater than a certain value [44]. This Courant limit is inversely proportional to the characteristic speeds of the system. We estimate allowable values for the Courant factor by examining the 2D wave equation in first order form, $\partial_t u_0 = \partial^i u_i$, $\partial_t u_i = \partial_i u_0$. Assuming second order, centered differencing for the spatial derivatives, we plot the Courant limits for third and fourth order Runge-Kutta as a function of the artificial dissipation parameter in Fig. 7.

The characteristic speeds in the cylindrical grid are bounded by 1 in magnitude. Looking at Fig. 7, this would suggest that one could use a Courant factor as large as 2.0 (using fourth order Runge-Kutta and ignoring the fact that this is a variable coefficient problem with lower order terms and with boundaries). However, in the spherical grid the characteristic speeds along the axis of symmetry

have a magnitude of

$$\sqrt{\frac{1+|\beta|}{1-|\beta|}}, \quad (99)$$

which is greater than 1 for $\beta \neq 0$. For example, for $\beta = 0.9$ the characteristic speeds in the spherical grid can be as large as $\sqrt{19} \approx 4.359$. In this case a Courant factor larger than ≈ 0.46 is likely to lead to numerical instability.

VII. NUMERICAL EXPERIMENTS

To our knowledge there are no stability proofs for two dimensional hyperbolic problems with overlapping grids. To check the convergence of our code we must rely on numerical experimentation.

Let $u(t, \vec{x})$ be the exact solution of the continuum problem and v_{ij}^n the solution of the fully discrete approximation. If, for any t , as $nk \rightarrow t$,

$$\epsilon_h^n \equiv (h_1 h_2 \sum_{ij} \|v_{ij}^n - u(nk, \vec{x}_{ij})\|^2)^{1/2} = \mathcal{O}(h^p) + \mathcal{O}(k^q)$$

as $k, h \rightarrow 0$, the difference scheme is said to be convergent of order (p, q) . This implies that the overall order of convergence of the scheme, assuming $k/h = \text{const.}$, is

$$Q \equiv \lim_{h \rightarrow 0} \log_2 \frac{\epsilon_h^n}{\epsilon_{h/2}^n} = \min\{p, q\} \quad (100)$$

as $nk \rightarrow t$, where t is some fixed time. To use this equation we must know an exact solution of the continuum problem.

Exact solutions for the scalar wave equation in Minkowski space are well known. To test our overlapping grid system we use spherical waves [45] given by

$$\Phi = \sum_{\ell} f_{\ell}(r) P_{\ell}(\cos \theta) e^{-i\omega t}, \quad (101)$$

where $P_{\ell}(\cos \theta)$ are the Legendre polynomials and we choose $f_{\ell}(r)$ to be the Hankel functions, which asymptotically represent in- and out-going waves. We tested the long-term behavior of our code by evolving an incoming spherical wave exact solution, and computing the norm of the error. These results are shown in Fig. 8.

When an exact solution is not available, which is often the case, the following standard technique of numerical analysis can be useful. Let w be an arbitrary function and let us rewrite the partial differential equation as $L(u) = 0$. If w is inserted into the equation, in general, it will produce a non vanishing right hand side,

$$L(w) = F. \quad (102)$$

Clearly, the modified equation $\tilde{L}(u) \equiv L(u) - F = 0$ has w as an exact solution and the convergence of the code can be tested using Eq. (100).

We chose $w(t, r, \theta) = \sin(t + r) \cos(n\theta)$, where $\{t, r, \theta\}$ are the spherical coordinates of the rest frame and n is an integer. This is an exact solution of

$$\nabla_\mu \nabla^\mu w - F = 0. \quad (103)$$

where F is given by

$$F = \frac{\cos n\theta}{r^2} (2r \cos(t + r) - n^2 \sin(t + r)) - n \frac{\sin n\theta}{r^2 \sin \theta} \cos \theta \sin(t + r). \quad (104)$$

Both w and F are scalar quantities. The evolution equation (31) is modified according to

$$\partial_t T = -(\gamma^{ti} \partial_i T + \partial_i (\gamma^{it} T) + \partial_i (\gamma^{ij} d_j) + \partial_t \gamma^{tt} T + \partial_t \gamma^{tj} d_j - \sqrt{-g} F) / \gamma^{tt}, \quad (105)$$

where $g = \det(g_{\mu\nu})$. On the axis of symmetry we use the limits $\lim_{\theta \rightarrow 0} \frac{\sin n\theta}{\sin \theta} = n$ and $\lim_{\theta \rightarrow \pi} \frac{\sin n\theta}{\sin \theta} = (-1)^{n+1} n$. The results of our convergence tests for different values of the boost parameter and $n = 2$ are summarized in Fig. 9. Movies are also available [46].

VIII. CONCLUSION

Systems with moving boundaries arise in a variety of situations, and their solution typically involves introducing coordinates adapted to the boundaries. These may be either a single, global coordinate system, such as those used in binary black hole evolutions [47, 48] that keep the black holes and the outer boundary at fixed coordinate positions, or, as advocated here, multiple coordinate patches. Whichever approach is adopted, fixing coordinates to the boundaries allows one to unambiguously specify proper boundary conditions, as required for well-posed problems. Moreover, boundaries at fixed grid coordinates eliminate the need for extrapolated data at points that emerge from a moving boundary.

In our model problem we have evolved an axisymmetric scalar field on a boosted Schwarzschild background. We used a cylindrical coordinate patch with respect to which the outer boundary is fixed, and we introduced an overlapping spherical coordinate patch co-moving with the hole. At any given time in the co-moving coordinate system the location of the inner boundary (the horizon) corresponds to a $r = \text{const.}$ surface. This surface can be represented exactly on the numerical grid and allows one to smoothly excise a large volume of spacetime, much larger than that permitted by cubical excision. Our numerical implementation made use of overlapping grids, where different but equivalent problems are solved on separate grids. To communicate data between grids we used interpolation on all fields.

The discrete version of the energy method, based on differencing operators that satisfy the summation by parts property, has demonstrated to be particularly effective for the construction of a stable discretization scheme

on the axis of symmetry, and for the identification of discrete boundary conditions. The stability proofs, which hold on individual grids, cannot be immediately extended to the overlapping grid scheme, due to the interpolation of data from one grid to another. We note, however, that it may be possible to define orthogonal projection operators for the interpolation that could allow to analytically demonstrate numerical stability [49]. This is a question of active interest. Nevertheless, our numerical tests indicate that our scheme is convergent, even for very high values of the boost parameter, and does not suffer from long term power-law or exponential growth in the error.

The model problem that we presented in this work is primarily intended as a proof of concept, and several avenues of research remain to be explored. Foremost might be the addition of the Einstein equations to the system for a dynamic black-hole spacetime, where the locations of the black hole singularity and event horizon are not a priori known. Depending on the dimensionality of the problem, one or more coordinate patches adapted to the inner boundary would have to be generated during evolution, along with the relationship between the various coordinate systems. By monitoring the characteristic speeds on the excision boundary (with respect to the coordinate system adapted to that boundary), one can guarantee its purely outflow properties, an essential requirement of excision.

Although alternative numerical approaches may be possible, the overlapping grid method has struck us for its strength and its simplicity. Owing to its flexibility in representing smooth, time dependent boundaries, we believe that this technique, or a similar one, will play a significant role in the solution of the binary black hole problem.

Acknowledgments

We thank Olivier Sarbach for many valuable discussions during this work, and for sharing early results on summation by parts for the two dimensional wave equation in axisymmetry. We thank Luis Lehner for sharing results of an earlier investigation of cubical excision in the Kerr spacetime, as well as for encouragement in the beginning phases of this project. We acknowledge Manuel Tiglio for interesting discussions and for providing Ref. [24]. We also thank N. Andersson, M. Choptuik, S. Liebling, P. Olsson, F. Pretorius, J. Pullin, O. Reula, and S. Teukolsky for helpful discussions. We thank L. Lehner and J. Pullin for comments on an earlier draft of this work and S. Ou for help with visualization. We acknowledge the hospitality of the Kavli Institute of Theoretical Physics at UCSB (DN), the Max-Planck-Institut für Gravitationsphysik (Albert-Einstein-Institut) and the University of Southampton (GC), where part of this research was done. This research was supported in part by the National Science Foundation under grants PHY-9907949 to the KITP and PHY-0244335 and

INT-0204937 to LSU, and the Horace Hearne Jr. Institute for Theoretical Physics.

Appendix

To gain some insight into the limitations of cubical excision and the consequent need for a smooth excision boundary, we consider the analytic Schwarzschild and Kerr solutions [20, 21]. We employ the commonly used Cartesian Kerr–Schild coordinates, which are smooth across the horizon, and write the metric as

$$g_{\mu\nu} = \eta_{\mu\nu} + 2H\ell_\mu\ell_\nu,$$

where $\eta_{\mu\nu}$ is the Minkowski metric, H is a scalar,

$$H = \frac{Mr}{r^2 + a^2 \cos^2 \theta},$$

and ℓ_μ is a null vector,

$$\ell_\mu = \left(1, \frac{rx + ay}{r^2 + a^2}, \frac{ry - ax}{r^2 + a^2}, \frac{z}{r} \right).$$

The parameter M represents the mass of the black hole and $J = aM$ is the total angular momentum. The spheroidal coordinates r and θ are given by

$$\cos \theta = \frac{z}{r}$$

$$r^2 = \frac{1}{2}(\rho^2 - a^2) + \sqrt{\frac{1}{4}(\rho^2 - a^2)^2 + a^2 z^2},$$

where $\rho^2 = x^2 + y^2 + z^2$.

We center a cube of side length $L = 2b$ on the black hole, $x^i \in [-b, b]$. In order to excise this region from the computational domain, we must ensure that its boundary is purely outflow, i.e., that no information can enter the computational domain. To determine the allowed values of b , we calculate the characteristic speeds on each face of the cube and check that the inequality $s_{\pm}^n \leq 0$, where \vec{n} is the outward unit normal to the boundary, is satisfied. The Schwarzschild solution is obtained by setting $a = 0$, and the calculation gives [20] $0 < b \leq 2\sqrt{3}/9M \approx 0.385M$. The calculations for Kerr ($a \neq 0$) are more involved, and we present our numerically generated results in Fig. 10. We find that because of the ring singularity ($\rho = a, z = 0$), in addition to a maximum size for the excision cube, there is also a *minimum* size. In addition, we notice that no cubical excision is possible for $a \gtrsim 0.0851M$. This is a severe constraint on the spin parameter, and precludes cubical excision for interesting values of spin. We note, however, that this limitation is coordinate dependent and that it might be possible to choose coordinates in which cubical excision may be done for higher values of a .

-
- [1] L. Lehner, *Class. Quantum Grav.* **18**, R25 (2001).
[2] L. Smarr and J. York, *Phys. Rev. D* **17**, 2529 (1978).
[3] D. Eardley and L. Smarr, *Phys. Rev. D* **19**, 2239 (1979).
[4] J.M. Bardeen and T. Piran, *Phys. Rep.* **196**, 205 (1983).
[5] M. Alcubierre, B. Brügmann, P. Diener, M. Kopptiz, D. Pollney, E. Seidel, and R. Takahashi, *Phys. Rev. D* **67** 084023 (2003).
[6] R. Wald, *General Relativity* (University of Chicago Press, Chicago, 1984).
[7] W. Unruh, quoted in J. Thornburg, *Class. Quantum Grav.* **4**, 1119 (1987).
[8] E. Seidel and W.-M. Suen, *Phys. Rev. Lett.* **69**, 1845 (1992).
[9] M.A. Scheel, S.L. Shapiro, and S.A. Teukolsky, *Phys. Rev. D* **51**, 4208 (1995).
[10] M. Alcubierre and B. Brügmann, *Phys. Rev. D* **63**, 104006 (2001).
[11] L. Kidder, M.A. Scheel, and S.A. Teukolsky, *Phys. Rev. D* **64** 064017 (2001).
[12] F. Pretorius, Ph.D. thesis, University of British Columbia, Vancouver, British Columbia, 2002.
[13] G. Calabrese, L. Lehner, D. Neilsen, J. Pullin, O. Reula, O. Sarbach, and M. Tiglio, *gr-qc/0302072*.
[14] Binary Black Hole Grand Challenge Alliance, *Phys. Rev. Lett.* **80**, 2512 (1998).
[15] S. Brandt, R. Correll, R. Gómez, M. Huq, P. Laguna, L. Lehner, P. Marronetti, R.A. Matzner, D. Neilsen, J. Pullin, E. Schnetter, D. Shoemaker, and J. Winicour, *Phys. Rev. Lett.* **85**, 5496 (2000).
[16] H. Yo, T.W. Baumgarte, and S.L. Shapiro, *Phys. Rev. D* **64**, 124011 (2001).
[17] D. Shoemaker, K.L. Smith, U. Sperhake, P. Laguna, E. Schnetter, and D. Fiske, *gr-qc/0301111*.
[18] U. Sperhake, K.L. Smith, B. Kelly, P. Laguna, and D. Shoemaker, *gr-qc/0307015* (2003).
[19] O. Reula, “Hyperbolic Methods for Einstein’s Equations,” *Living Rev. Relativity* **1**, 3 (1998). [Online article]: cited on 31 July 2003, <http://www.livingreviews.org/lrr-1998-3>.
[20] M. Scheel, Talk at Miniprogram on Colliding Black Holes: Mathematical Issues in Numerical Relativity, Institute for Theoretical Physics, University of California at Santa Barbara, January 10–28, 2000. Available at <http://online.kitp.ucsb.edu/online/numrel00>
[21] L. Lehner, private communication (2003).
[22] A. Pfeiffer, L. Kidder, M. Scheel, S. Teukolsky, *Comput. Phys. Commun.* **152** 253-273 (2003).
[23] A. Dadone and B. Grossman, *AIAA Journal* **32**, 285 (1994).
[24] F. Bassi and S. Rebay, *J. Comput. Phys.* **138**, 251 (1997).
[25] S. Husa, private communication (2003).
[26] L. Lehner, M. Huq, and D. Garrison, *Phys. Rev. D* **62**, 084016 (2000).
[27] B. Gustafsson, H. Kreiss, and J. Olinger, *Time dependent*

- problems and difference methods* (John Wiley & Sons, New York, 1995).
- [28] Some recent examples of numerical relativity studies in axisymmetry include: M.W. Choptuik, E.W. Hirschmann, S.L. Liebling, and F. Pretorius, gr-qc/0305003 (2003); F. Siebel, J.A. Font, E. Müller, and P. Papadopoulos, gr-qc/0301127 (2003); M. Shibata, Phys. Rev. D **67**, 024033 (2003); M.W. Choptuik, E.W. Hirschmann, S.L. Liebling, and F. Pretorius, Class. Quant. Grav. **20**, 1857 (2003); J. Frauendiener, Phys. Rev. D **66**, 104027 (2002); H. Dimmelmeier, J.A. Font, and E. Müller, Astron. Astrophys. **393**, 523 (2002); H. Dimmelmeier, J.A. Font, and E. Müller, Astron. Astrophys. **388**, 917 (2002); F. Siebel, J.A. Font, E. Müller, and P. Papadopoulos, Phys. Rev. D **65**, 064038 (2002); H. Dimmelmeier, J.A. Font, and E. Müller, Astrophys. J. **560**, L163 (2001); J.A. Font, H. Dimmelmeier, A. Gupta, and N. Stergioulas, Mon. Not. Roy. Astron. Soc. **325**, 1463 (2001); M. Alcubierre, B. Brügmann, D. Holz, R. Takahashi, S. Brandt, E. Seidel, and J. Thornburg, Int. J. Mod. Phys. D **10** 273 (2001); M. Shibata, Prog. Theor. Phys. **104**, 325 (2000); D. Garfinkle and G.C. Duncan, Phys. Rev. D **63**, 044011 (2001); S. Brandt, J.A. Font, J.M. Ibañez, J. Massó, and E. Seidel Comput. Phys. Commun. **124**, 169 (2000); P. Papadopoulos and J.A. Font, Phys. Rev. D **58**, 024005 (1998); P. Anninos, S.R. Brandt, and P. Walker, Phys. Rev. D **57**, 6158 (1998); S. Bonazzola, J. Friebe, and E.ourgoulhon, Ap. J. **460**, 379 (1996); M. Bocquet, S. Bonazzola, E.ourgoulhon, and J. Novak, Astron. Astrophys. **301**, 757 (1995); P. Anninos, D. Hobill, E. Seidel, L. Smarr, and W.-M. Suen, Phys. Rev. D **52**, 2044 (1995); R. Gomez, P. Papadopoulos, and J. Winicour, J.Math.Phys. **35**, 4184 (1994); P. Anninos, D. Hobill, E. Seidel, L. Smarr, and W.-M. Suen, Phys. Rev. Lett. **71**, 2851 (1993).
- [29] P. Olsson, Math. Comp. **64**, 1035 (1995); **64**, S23 (1995); **64**, 1473 (1995).
- [30] O. Sarbach, in preparation.
- [31] G. Starius, Numer. Math. **35**, 241-255 (1980).
- [32] G. Chessire and W.D. Henshaw, J. Comput. Phys. **90**, 1 (1990).
- [33] H.-O. Kreiss and J. Olinger, *Methods for the approximate solution of time-dependent problems*, GARP Publication Series No. 10 (World Meteorological Organization, Geneva, 1973).
- [34] G. Calabrese and O. Sarbach, gr-qc/0303040
- [35] F. Olsson and N.A. Petersson, Computers and Fluids **25**, 583 (1996).
- [36] J. Thornburg, Class. Quantum Grav. **4**, 1119 (1987); gr-qc/0012012 (2000); gr-qc/0306056 (2003); in preparation (2003).
- [37] B. Strand, J. Comput. Phys. **110**, 47 (1994)
- [38] G. Calabrese, L. Lehner, O. Reula, O. Sarbach, and M. Tiglio, gr-qc/0308007 (2003).
- [39] L. Lehner, D. Neilsen, O. Reula, and M. Tiglio, in preparation.
- [40] H.O. Kreiss, J. Lorenz, *Initial-Boundary Value Problems and the Navier-Stokes Equations* (Academic Press, Boston, 1989).
- [41] P.D. Lax, and R.S. Phillips, Commun. Pure Appl. Math. **13**, 427 (1960).
- [42] R. Arnowitt, S. Deser, and C. Misner, in *Gravitation: An Introduction to Current Research*, edited by L. Witten (Wiley, New York, 1962).
- [43] R.P. Kerr and A. Schild in *Comitato Nazionale per le Manifestazioni Celebrative del IV Centenario della Nascita di Galileo Galilei, Atti del Convegno sulla Relatività Generale: Problemi dell'Energia e Onde Gravitazionali*, 1–12, edited by G. Barbéra, Florence, (1965); R.P. Kerr and A. Schild, in *Proceedings of Symposia in Applied Mathematics* **17**, 199, American Math. Soc. (1965).
- [44] R. Courant, K.O. Friedrichs, and H. Lewy, Math. Ann. **100**, 32 (1928).
- [45] J.D. Jackson, *Classical Electrodynamics* 3rd. Edition (John Wiley, New York, 1999).
- [46] <http://relativity.phys.lsu.edu/movies/axisymmetry>
- [47] M. Alcubierre, B. Brügmann, D. Pollney, E. Seidel, and R. Takahashi, Phys. Rev. D **64**, 061501 (2001).
- [48] M. Alcubierre, W. Bengert, B. Brügmann, G. Lanfermann, L. Nerger, E. Seidel, and R. Takahashi, Phys. Rev. Lett. **87** 271103 (2001).
- [49] P. Olsson, private communication (2003).

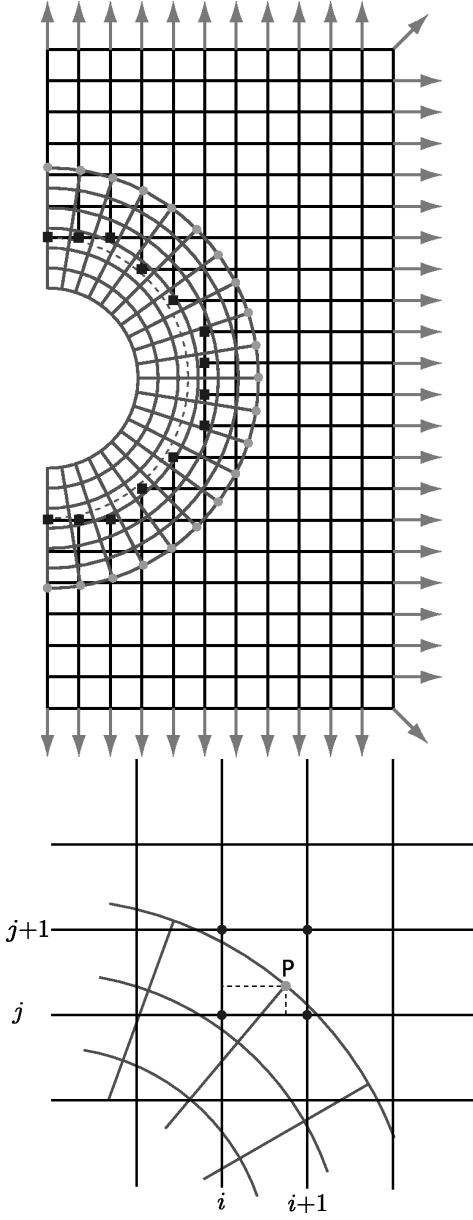


FIG. 6: The first figure shows the overlapping grids for the axisymmetric wave equation on a boosted black hole background. The spherical grid is used to excise the black hole from the computational domain. The dashed line represents a $r' = \text{const.}$ curve on the spherical patch. This is where the cylindrical coordinate system terminates. The arrows on the outer boundary indicate how the unit normal is chosen at each boundary grid point where boundary data must be specified. The circles and the square are used to mark points of the spherical and cylindrical grid respectively which are updated through interpolation. As shown in the second figure, the value of the fields on the grid point P of the spherical grid are computed by interpolating the values of the fields on the four neighboring points.

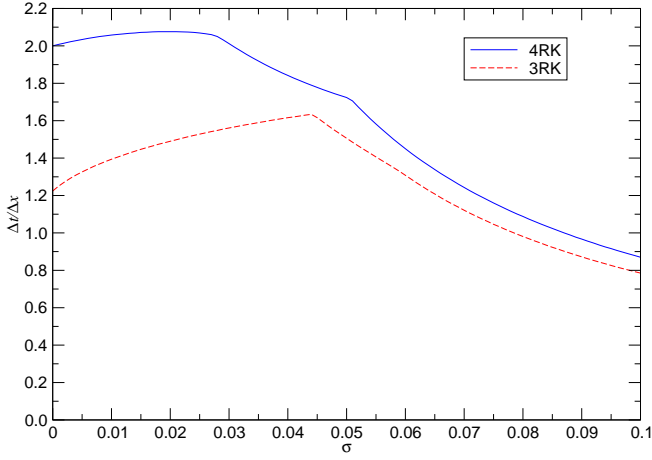


FIG. 7: The Courant limits for the 2D first order wave equation $\partial_t u_0 = \partial^2 u_i$, $\partial_t u_i = \partial_i u_0$ for fourth order (4RK) and third order Runge-Kutta (3RK). The calculation assumes no boundaries and second order centered difference operators for the approximation of the spatial derivatives. The value of σ represents the amount of artificial dissipation, $-\sigma \sum_{i=1}^2 h_i^3 (D_+^{(i)} D_-^{(i)})^2 u$, added to the rhs of the equations.

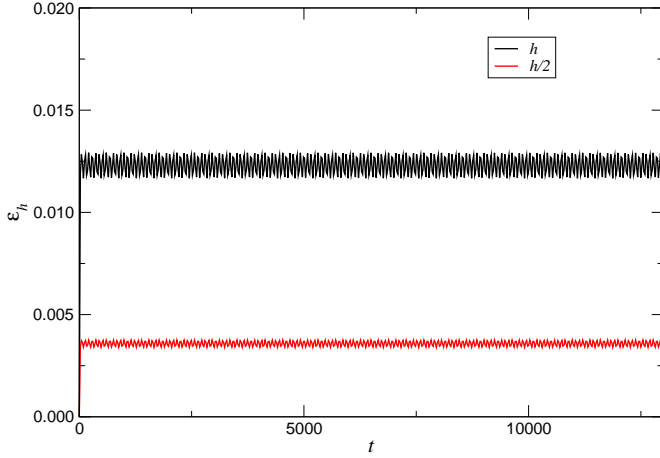


FIG. 8: These long term runs done at a fairly coarse resolution for $\beta = M = 0$ suggest that the interpolation between the overlapping grids does not introduce any power law or exponential growth. Here the exact solution is given by the the real part of the $\ell = 0$ mode with $\omega = 2$, with the in-going Hankel function for the radial variable in Eq. (101). The dissipation parameter is set to $\sigma = 0.02$. The ranges of the dependent variables are $0 \leq \rho \leq 10$, $-10 \leq z \leq 10$, $1 \leq r \leq 5$, and $0 \leq \theta \leq \pi$. The coarsest resolutions for the cylindrical and spherical grids are 90×170 and 50×68 , respectively.

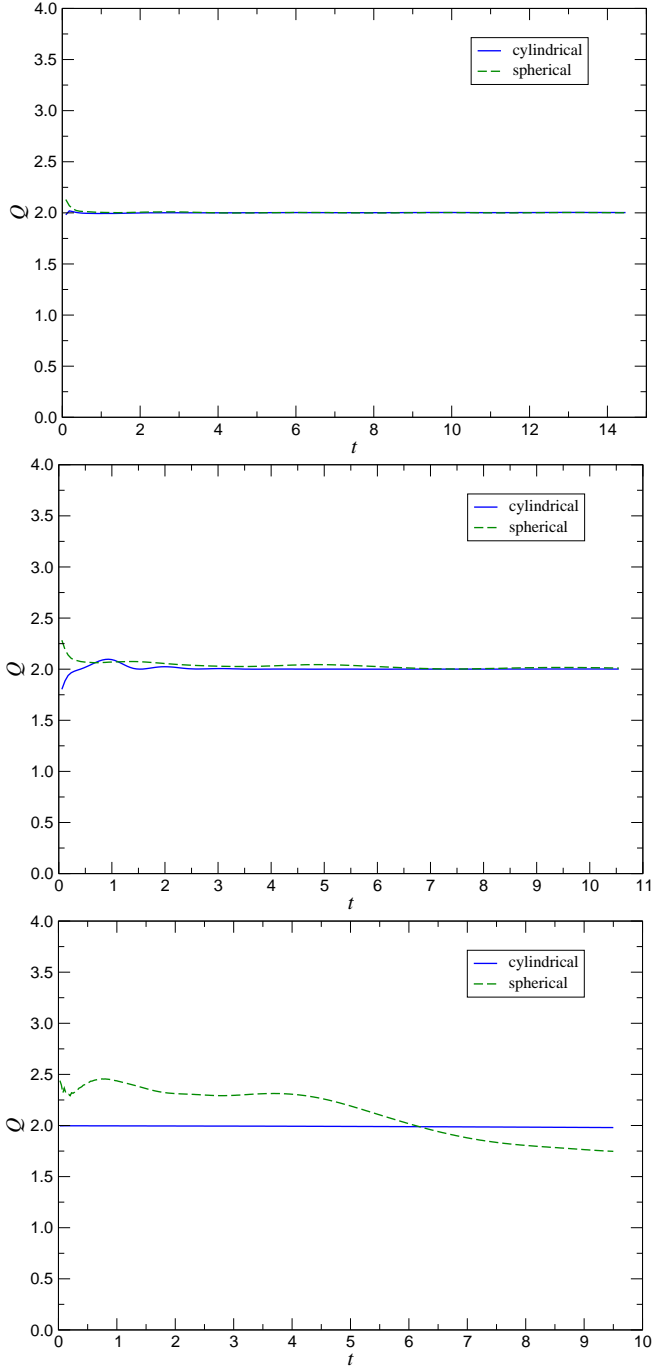


FIG. 9: In these figures we plot the convergence factor $Q(t) = \log_2(\epsilon_h^n / \epsilon_{h/2}^n)$ as a function of $t = nk$ for a sufficiently small value of the spacing h . The convergence test was carried out with the modified system (105) for boosting parameters $\beta = -0.5, -0.75,$ and -0.95 , from top to bottom, suggesting that the equations are correctly implemented and that the overall scheme is second order accurate. The resolutions used in the cylindrical and spherical grid are 256×512 , 128×384 and 512×1024 , 256×768 . The domain extends from $-10M$ to $+10M$ in the \bar{z} direction and up to $+10M$ in the $\bar{\rho}$ direction. The spherical patch covers the region $2M \leq r' \leq 3M$. We used a Courant factor of 1.15, 0.75, and 0.32, and a dissipation parameter of $\sigma = 0.02$. The evolution is stopped just before the spherical grid touches the outer boundary of the cylindrical grid. In the $\beta = -0.95$ the system is only strongly hyperbolic at the bottom right corner of the cylindrical grid. We found that, to achieve convergence, we must give data to all fields at this point.

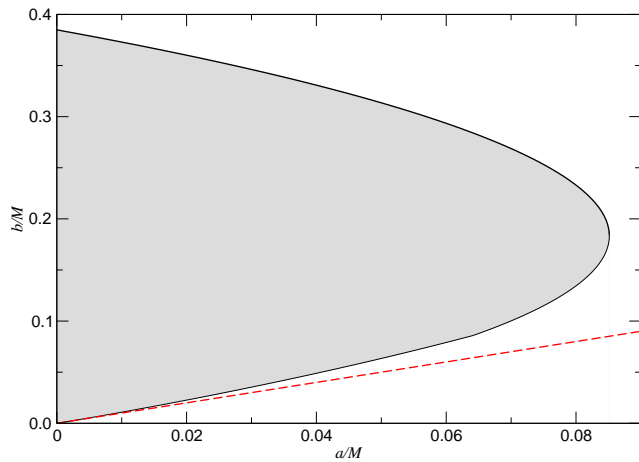


FIG. 10: This figure indicates the limitations of cubical excision in the Kerr spacetime in rectangular Kerr–Schild coordinates. We assume that the excision cube is centered on the hole, and that the faces of the cube are at $\pm b$. (See description in text.) Values of b for which an inner boundary has no incoming modes, and thus a candidate for an excision boundary, are indicated by the shaded region in the figure. The structure of the Kerr spacetime results in both maximum and minimum limits to the size of the excision cube. We find that, in this particular coordinate system, cubical excision for Kerr is well-defined only for very small spin parameters, $a \lesssim 0.0851M$, where $a = J/M$. For values of b below the dashed line, the excision cube intersects the ring singularity.